University of Zurich[UZH]

Wood anatomical response of Fokienia hodginsii to climate in Vietnam

GEO 511 Master's Thesis

Author
Silvia Passardi
14-727-515

Supervised by
Prof. Dr. Paolo Cherubini (paolo.cherubini@wsl.ch)
Dr. Brendan M. Buckley (bmb@ldeo.columbia.edu)

Faculty representative
Prof. Dr. Markus Egli

29.09.2020
Department of Geography, University of Zurich

University of Zurich[UZH]

Department of Geography

Wood anatomical response of *Fokienia hodginsii* to climate in Vietnam

GEO 511 Master's Thesis

Author

Silvia Passardi

14-727-515

Supervised by

Prof. Dr. Paolo Cherubini	Swiss Federal Institute for Forest, Snow and Landscape Research (WSL)
Dr. Brendan M. Buckley	Lamont-Doherty Earth Observatory (LDEO), Columbia University

Faculty representative

Prof. Dr. Markus Egli	University of Zürich (UZH)

September 2020

Department of Geography, University of Zurich

Abbreviations

%LA	percent total lumen area
ALA	average lumen area
ALL	average lumen length
ALP	average lumen perimeter
ALLW	average lumen length/width
ALW	average lumen width
AFC	average form coefficient
AMJ	April-May-June
ASM	Asian summer monsoon
ASO	August-Septeber-October
BI	blue intensity
ΔBI	difference between EWBI and LWBI
DJF	December-January-February
eACL	average cell length of EW cells
eAFC	average form coefficient of EW cells
eALA	average lumen area of EW cells
eALL	average lumen length of EW cells
eALP	average lumen perimeter of EW cells
eALLW	average lumen length/width of EW cells
eALW	average lumen width of EW cells
eAWT	average wall thickness of EW cells
ENSO	El Niño-Southern Oscillation
EW	earlywood
EWBI	earlywood blue intensity
FMA	February-March-April
IPO	Interdecadal Pacific Oscillation
IUCN	International Union for Conservation of Nature
JAS	July-August-September
JFM	January-February-March
JJA	June-July-August
lACL	average cell length of LW cells
lAFC	average form coefficient of LW cells
lALA	average lumen area of LW cells
lALL	average lumen length of LW cells
lALP	average lumen perimeter of LW cells
lALLW	average lumen length/width of LW cells
lALW	average lumen width of LW cells
lAWT	average wall thickness of LW cells
LDEO	Lamont–Doherty Earth Observatory of Columbia University in New York
LW	latewood
LWBI	latewood blue intensity
MAM	March-April-May
MJJ	May-June-July
MSI	mean series intercorrelation
MXD	maximum latewood density
NCSs	non-structural carbohydrates
NDJ	November-December-January
OND	October-November-December (of the previous year)
PDSI	Palmer Drought Severity Index
RW1	ring width based on LDEO measurements
RW2	ring width based on WSL measurements
SON	September-October-November (of the previous year)
SPEI	Standardized Precipitation Evapotranspiration Index
WSL	Swiss Federal Institute for Forest, Snow and Landscape Research

Abstract

The classical paradigm on tropical dendrochronology said that trees growing in tropical areas were not reliable for paleo-ecological and climatological studies because of their lack of clear annual rings. The dendrochrological studies carried out in the last decades have instead shown that some species have annual tree rings and therefore this paradigm is being overcome. Among these species there is the *Fokienia hodginsii*, a conifer for which several chronologies have been developed that have allowed to reconstruct climatic parameters.

The aim of this master thesis is to explore the potential of wood anatomy for climate reconstruction and for a better understanding of the present climate of Southeast Asia. Microslides were produced from cores of *Fokienia hodginsii* from Central Vietnam, they were scanned and the images were analysed using the software WinCELL. The resulting anatomical data were analysed in comparison with climatic data.

The results are promising: the anatomical parameters correlate better with maximum temperature, precipitation and the Standardized Precipitation Evapotranspiration Index than ring width does. The results support the hypotheses of other studies on climatic conditions that affect *Fokienia hodginsii* xylem growth. Among the various anatomical parameters measured, those that have the strongest climate responses are average lumen perimeter and average lumen length. Since the anatomical characteristics have also been studied by dividing the cells into earlywood and latewood cells, this research gives the first insights at the intra-annual time scale into the growth of the tree rings.

Introduction

Dendrosciences

Dendrochronology is defined as the science of dating annual tree rings (Kaennel & Schweingruber, 1995). Tree rings are growth layers of the woody tissue (xylem) of a plant. Tree rings are formed by the cell division of the cambium. The cells that form the woody tissue that carries water and nutrients upwards and mechanically supports the plant (xylem) are formed inwardly, while the cells of the tissue that carries processed nutrients downwards (phloem) are formed outwardly. At the beginning of the growing season, which in temperate climates is the spring, in conifers cells with large lumens and fine cell walls are formed. These cells mainly have the function of transporting water and nutrients upwards and form a tissue called earlywood (EW). During the summer, cells grow smaller and with thicker cell walls to mechanically support the tree. These cells are called latewood (LW) cells (Fritts, 1971). Because of anatomical differences between EW and LW cells, tree rings are visible even at a macroscopic level as an alternation of darker and lighter growth layers (Figure 1).

The amount of wood that a plant can produce in a vegetative period depends on several factors, which can be both endogenous (e.g., type of species) and exogenous (e.g., climatic and ecological disturbances). Dendrochronological methods can therefore be used to reconstruct past climatic conditions (dendroclimatology) or local ecological disturbances (dendroecology). If past environmental conditions are known, the growth analysis may provide information on the physiological reaction of the tree to environmental conditions (Fritts, 1971).

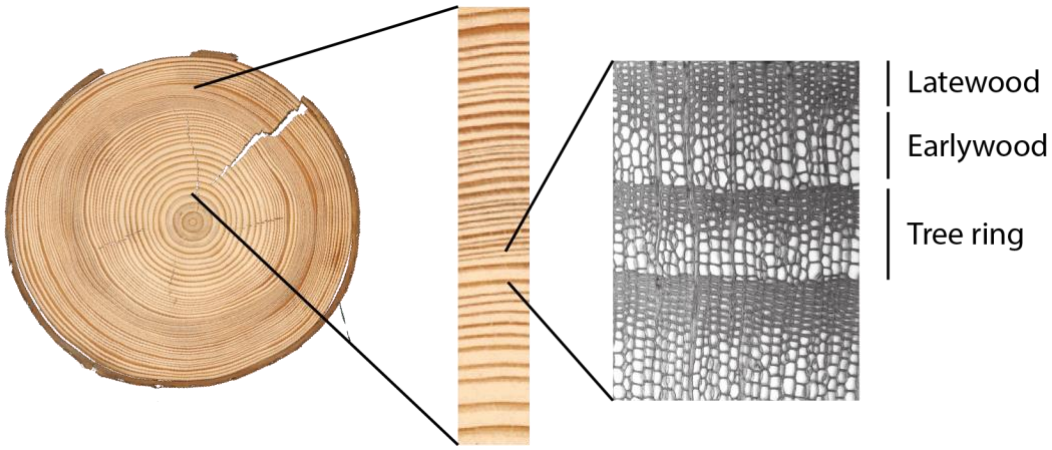

Figure 1: Tree disk, tree core and anatomical detail (own editing of images of Holger Gärtner, WSL).

Although Leonardo da Vinci in the 15th century had already observed a relationship between rainfall and tree rings, the father of dendrochronology is considered to be the American astronomer Andrew Ellicott Douglass. He began his studies on tree rings in 1901. He hypothesized that tree rings are a climate proxy and noted similar trends in the growth of trees that grew in sites with different climates, and he started to match

the variations in ring width among several tree ring series. This process is now known as cross dating and was established in 1904. In the following decades, tree ring research was mainly used to date archaeological finds. Since the 1940s, the study of tree rings has been applied to climate research (Robinson, 1990). Beginning in the 1940s, dendrochronology began to spread throughout Europe thanks to the German botanist Bruno Huber. In the 1960s, modern statistical methods were introduced to support dendroclimatology, the study of wood density by X-ray began and xylem anatomical characteristics had started to be researched (Eckstein, 2013; Schweingruber, 1988). The latter are not only a means for the identification and classification of the species but can also be used as climatic proxies to reconstruct ecological disturbances or to understand the physiology of the tree (Crivellaro & Schweingruber, 2013).

The set of cells of which the trunk is composed performs numerous vital functions for the existence of the plant, even while the trunk grows (Crivellaro & Schweingruber, 2013). Since the beginning of the evolution of land plants, xylem has had to perform multiple functions, such as water transport, mechanical support and storage of water and nutrients. In the course of evolution, xylem cells have always faced this trade-off, even in the context of a changing climate (Baas, Ewers, et al., 2004; Baas & Wheeler, 2011). The wood anatomy therefore represents both a very long evolutionary path and the ecological and climatic conditions of the moment in which the cells grew. By analysing the anatomy, it is possible to obtain data at an intra-annual level (Von Arx et al., 2016).

Dendrochronology and dendroecology in tropical regions

In temperate climates, where the growing season is followed by a dormant season, tree rings are usually formed annually. Trees are in growing conditions for only a few summer months, while during the winter, the growth stops due to severe weather conditions. Until a few decades ago, the classical paradigm on tropical dendrochronology said that trees growing in tropical areas were not reliable for paleo-ecological and climatological studies because of their lack of clear annual rings (Buckley et al., 2017; Cherubini et al., 2003). However, if there is a triggering climate factor once a year, rings can form annually. In the case of tropical regions, the temperature usually remains constant, but precipitation is concentrated over the year. The annuality of the rings can be proven by different methods: phenological observations, cambial wounding, radiocarbon dating, observations of extreme climatic or environmental events and successful correlation of tree ring time series with climate records (Worbes & Fichtler, 2010).

Pumijumnong (2013) reviewed the development of dendrochronology in Southeast Asia. In 1931, an initial chronology had already been published by Berlage (Pumijumnong, 2013). The growth of Java teak in this first chronology shows a correlation with rainy days. The chronology was subsequently revised and expanded, but for a long period, teak was the only tree considered promising for dendrochronology in tropical and subtropical Southeast Asia. Between 1995 and 2011, teak remained an important object of research, but

other species also began to be studied. Among these, *Pinus merkusii* and *Pinus kesiya* have given promising results despite their high production of resin and their susceptibility to natural and human-driven fires, which can strongly influence the correlations between pine ring width and climate data (Pumijumnong, 2013).
After 2008, the first studies on *Fokienia hodginsii* were also published. As will be discussed in more detail in the next chapter, this conifer has allowed for valid hydroclimatic reconstructions. In addition to the classic dendrochronological research, mainly based on the correlations between climate and ring width, research also began after 1995 on wood anatomical features and the monitoring of cambial activity. These two recent approaches help to date even species that do not have clear annual rings. Stable oxygen and carbon isotope ratio measurements began to be used to study climate variability and to date tropical trees (Pumijumnong, 2013).
The paradigm that said that dendrochronological methods are not applicable in regions with tropical climates is therefore being overcome. Asian dendrochronology has expanded tremendously since the year 2000 with the establishment of several new laboratories and the publication of many tree ring chronologies, which considerably increase both spatially and temporally the availability of tree ring data (Linderholm et al., 2013).

Dendrochronological studies in subtropical and tropical Asia are made particularly difficult not only by the absence of a clear seasonality but also by the recent history of forests, which includes great destruction due to intense logging (Pumijumnong, 2013) and wars (Robert, 2016). Particularly in Vietnam, the war between 1955 and 1975 had very serious consequences for the environment: 72 millions litres of herbicides (including Agent Orange) in high concentrations were sprayed from the air (Lamb, 1985), bulldozers were in action and fire was applied to destroy the canopy cover and crops, which enemies could hide under and feed upon (Robert, 2016). Bombings (including incendiary bombings with Napalm) and the need to create infrastructures and communication pathways during the war caused deforestation and environmental destruction (Robert, 2016). According to Lamb (1985), during the Vietnam War, two million hectares of forest were destroyed in what was South Vietnam (and about 200,000 hectares in North Vietnam). The destruction of the landscape has had devastating side effects, such as the loss of habitat for many plants and animals, some of which have become extinct, and increased erosion, flooding and landslides (Lamb, 1985).
In addition to these difficulties, the lack of climatological records makes it more difficult to carry out dendroclimatological studies in Southeast Asia (Sano et al., 2009).

Climate in Vietnam

The Asian continent is mainly characterized by cold or arid climates according to the Köppen–Geigen classification (cold and arid climates being represented by the letters D and B, respectively). In Southeast Asia, however, a tropical climate (A) prevails (Figure 2). The criterion that defines the macro-category of

tropical climates says that their coldest month's temperature should be greater than or equal to 18°C (Peel et al., 2007).

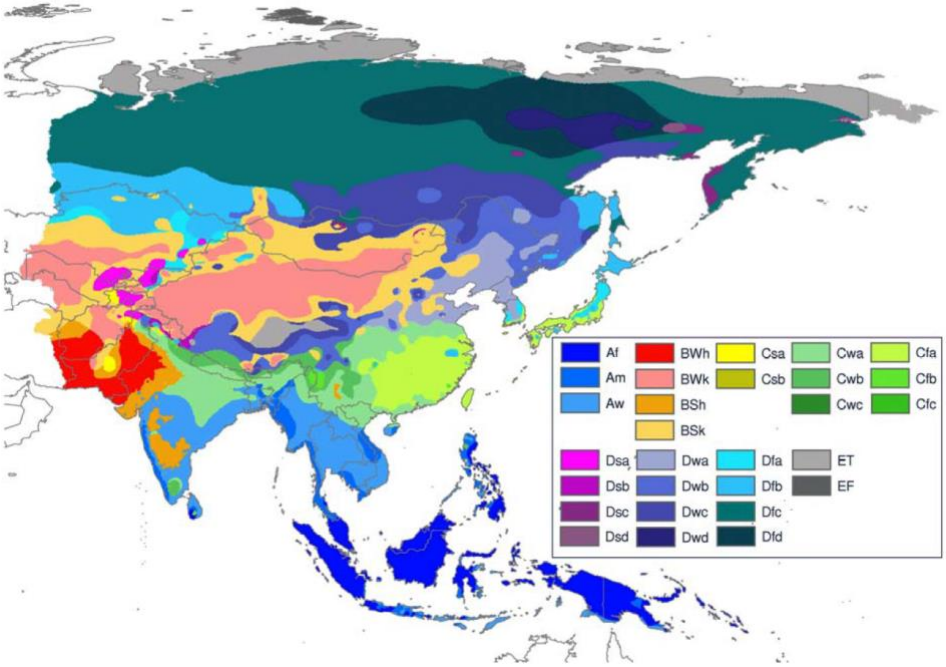

Figure 2: Köppen–Geiger climate type map of Asia (Peel et al., 2007).

Vietnam is a small country (less than 330,000 km^2) that extends longitudinally for over 1600 km and contains coastal and mountainous areas; consequently, the climate is not the same in all regions of the country (Nguyen-Le et al., 2014).

In Central Vietnam, where the principal sample site of this research is located, the average temperature varies between 20°C and 30°C during the year. Since the average temperature in January (the coldest month) is 21°C, this climate is defined as tropical. The region's maximum temperatures are reached during the summer months June-July-August (29°C). Rainfall varies much more than temperature throughout the year: from January to August, it rains less than 200 mm per month, while in the remaining four months, it rains up to over 600 mm per month (Figure 3; Deutscher Wetterdienst, 2020). Due to this distribution of precipitation during the year, the climate of the Da Nang climate station is classified as tropical monsoon (Am) according to the Köppen–Geiger classification. This type of climate is mainly found in Central Vietnam, while the South has a tropical savannah climate (Aw) and the North a temperate climate with hot and dry summers (Csa; Peel et al., 2007).

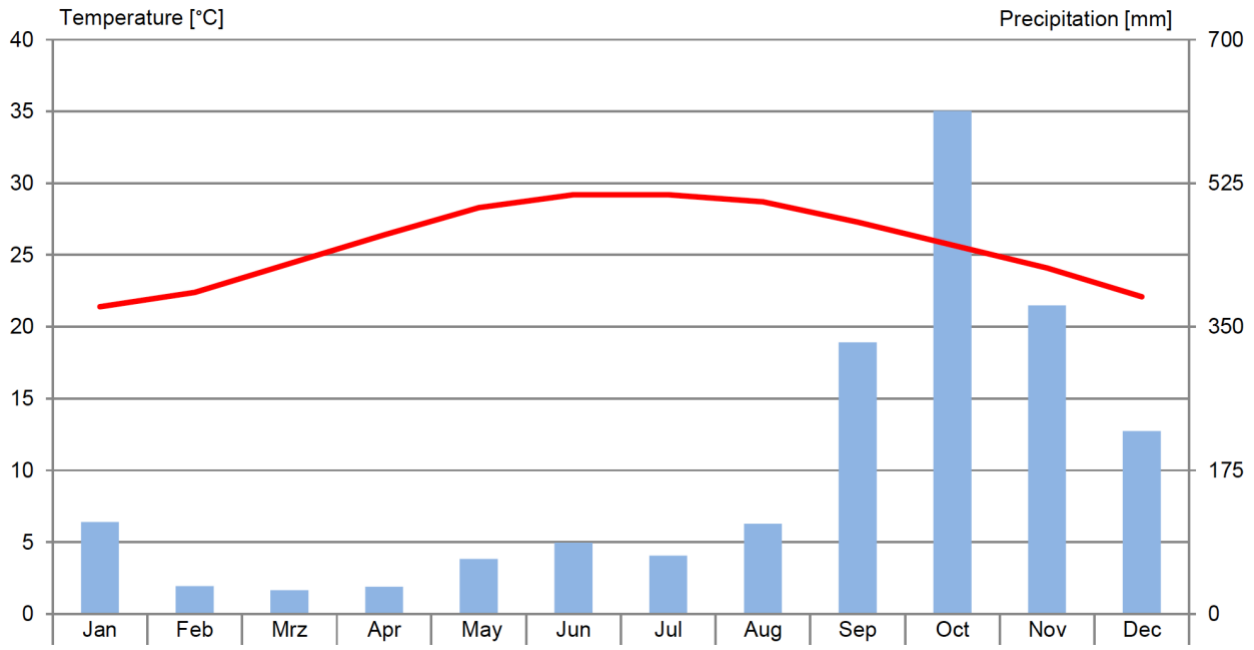

Figure 3: Climate diagram of the weather station of Da Nang (16° 02' N, 108° 11' E, 1941-1970; translated from Deutscher Wetterdienst, 2020).

The precipitation in Vietnam, as well as in a large part of the Asian continent, is driven by the Asian summer monsoon (ASM; Buckley et al., 2017), which is the largest and strongest monsoon system in the world (Liu et al., 2019). The ASM is a phenomenon of atmospheric circulation due to the thermal difference between sea and land (Liu et al., 2019).

The ASM affects the various regions of Southeast Asia differently. The climatological ASM onset date for the Indochina Peninsula (the mainland of Southeast Asia) was determined to be 9 May (Nguyen-Le et al., 2014). However, in Central Vietnam, the ASM behaves very differently than in most of Southeast Asia. In Central Vietnam, the wet season starts not at the beginning of summer but in autumn (September–November). This difference is caused by the orography of Central Vietnam, by cold surges and by tropical disturbances over the South China Sea in early winter. During the summer, the climate in Central Vietnam is rather dry because of foehn winds, which are caused by the ASM. Most of the rain falls on the windward slopes in Laos and Cambodia. The rain that falls in autumn comes from the South China Sea and is brought to Central Vietnam by winter monsoon westerlies (Nguyen-Le et al., 2014).

The rhythm of the annual rains and drought affects the rhythm of activities of human society, such as agriculture, forestry and fishing (Buckley et al., 2014; Nguyen-Le et al., 2014). Although the understanding of monsoons is so important for social and economic activities, there are still knowledge gaps (Nguyen-Le et al., 2014). Understanding the dynamics that cause the distribution in space and time of rainfall, floods and droughts in Southeast Asia in the context of climate change plays a crucial role in the social and economic development of the region (Liu et al., 2019).

The ASM is not the only climatic pattern affecting Southeast Asia: several coupled ocean–atmosphere modes affect the climate of that area and interact with the ASM (Zheng, 2019). The two main climate modes that interact with the ASM are the El Niño–Southern Oscillation (ENSO) and the Interdecadal Pacific Oscillation (IPO), but the North Atlantic sea surface temperature, Indian Ocean Dipole and Eurasian snowpack anomalies are also part of the climatic phenomena related with the ASM (Buckley et al., 2014).

The ENSO is a recurring climate pattern that is active across the tropical Pacific and that disrupts large-scale air movements in the tropics, which affect the global climate. The ENSO is formed by two phase events: El Niño (warm-phase events) and La Niña (cool-phase events). The change between the two phases can take place every two to seven years (*El Niño-Southern Oscillation (ENSO)*, n.d.). The influence of ENSO on the regional climate varies greatly both spatially and temporally in Southeast Asia (Räsänen et al., 2016). In general terms, El Niño manifests itself in Vietnam with droughts in the early monsoon season, whereas La Niña corresponds with increased early monsoon moisture (Buckley et al., 2017).
The IPO is a trans-Pacific sea surface temperature anomaly pattern that is directly correlated with the decadal trend of the ENSO phenomenon. The IPO influences the Pacific climate and beyond. Of this climate mode, only the observations of three phases (in the 20th century) and a small number of reconstructions are available (Buckley et al., 2019).

Fokienia hodginsii

The tree species *Fokienia hodginsii* belongs to the phylum Tracheophyta, the class Pinopsida and the order Pinales (Thomas & Yang, 2013). It is a genus of conifer belonging to the Cupressaceae family (subfamily Cupressoideae), most commonly known as the family of cypresses. According to the International Union for Conservation of Nature (IUCN), the official name of the species has changed and is now *Chamaecyparis hodginsii* and no longer *Fokienia hodginsii* (Thomas & Yang, 2013). The name change is due to molecular analysis showing that *Fokienia* clusters with *Chamaecyparis* (Rushforth, 2014). According to Rushforth (2014), the morphological characters of *Fokienia* also do not differ significantly from those of *Chamaecyparis* and therefore the existence of two distinct genera is not justified. However, in this thesis, the name *Fokienia* is retained since it is still more common in the scientific literature. C*upressus hodginsii* is another name for the same species. In English, the common name is Fujian cypress and in Vietnamese is Po mu (Thomas & Yang, 2013).

Figure 4: Leaves, trunk and bark detail of Fokienia hodginsii.

This species is typically a minor component of subtropical-to-warm temperate evergreen (mixed) mesophytic forest between 300 and 2,300 m above sea level (masl) that receives at least 1,500 mm of precipitation per year and has loamy sand soil with a pH of 5–6 (Thomas & Yang, 2013). *Fokienia hodginsii* is an evergreen tree that can be up to 35 m high and can reach a diameter at breast height of 200 cm. Its crown has a pyramidal shape and its bole is straight. Its bark is grey-brown in colour and dries and cracks longitudinally (Figure 4, right). Its leaves are scale-like and are arranged in tripinnate branchlet systems (Figure 4, left). Male cones are oval to cylindrical, about 2.5 mm long and with 3–5 pairs of scales. Female cones are similar to those of other *Chamaecyparis* species and larger than male ones (about 25 mm long and 22 mm wide and composed of 5–8 pairs of scales). They ripen in the second year and two seeds grow on each scale. *Fokienia hodginsii* is a very long-living plant (Dallimore et al., 1967).

Fokienia hodginsii is native to southern China, Laos and Vietnam (Thomas & Yang, 2013). The genus *Fokienia* (when it is considered a genus) is monotopic, meaning it counts only a living species, which is *Fokienia hodginsii* (Román-Jordán et al., 2017).

This plant was categorized as vulnerable by the IUCN Red List of the Threatened Species in 2010; it was previously categorized in 1998 as lower risk and near threatened and as rare. *Fokienia hodginsii* has been judged to be vulnerable despite the fact that there are no reliable data on the decrease in the number of individuals, but it is assumed that that number has decreased by at least 30% over the last three generations (more than 300 years). In China, *Fokienia hodginsii* is relatively common; in fact, it is estimated that there are more than 650,000 individuals there, while in Vietnam and Laos, the subpopulations are fragmented and localized. In China, *Fokienia hodginsii* also grows even when planted (in parks and cemeteries), while outside of Laos, China and Vietnam, it is very rare even planted. In Laos and Vietnam, *Fokienia hodginsii* subpopulations are decreasing due to legal and illegal logging, even in national parks. Because of its

characteristics, this genus's wood is particularly coveted for the construction of coffins, doors, window frames, carved panels and furniture (Thomas & Yang, 2013).

According to Buckley et al. (2017), *Fokienia hodginsii* is the only tree species that grows in tropical Asia from which it has been possible to reconstruct climatic parameters that pass calibration-verification procedures. This species is particularly suitable for dendroclimatological studies because it builds annual tree rings and because of its longevity and sensitivity to moisture. From this species have been derived the most robust Southeast Asian tree ring chronologies (Buckley et al., 2017).
More knowledge of *Fokienia hodginsii*'s ecology (as for other threatened tropical tree species) is necessary in order to implement effective conservation policies (Zuidema et al., 2011).

Dendrochronological studies on *Fokienia hodginsii*

So far, five dendrochronological records of Vietnamese *Fokienia hodginsii* have been published.
The first chronology (MCFH) was published by Sano et al. in 2009 and, besides being the first chronology of *Fokienia hodginsii*, was at that point the longest cross dated tree ring chronology for continental Southeast Asia and the first chronology of any species in Vietnam. This chronology (1470–2004 AD) is based on 42 cores of 22 trees growing in the Mu Cang Chai area (1,700 masl) in Northern Vietnam. With this chronology, it was possible to reconstruct the Palmer Drought Severity Index (PDSI), which gives insights about soil moisture availability (Sano et al., 2009).
The second chronology (BDFH, 1030–2008 AD) is based on trees growing at two sites in the highlands of Vietnam's Bidoup Nui Ba National Park (Southern Vietnam) and was published by Buckley et al. in 2010. With this chronology, the early monsoon PDSI was reconstructed for the years 1250–2008 AD (Buckley et al., 2010).
In 2012, Sano et al. published a $\delta^{18}O$ chronology for the past 300 years (1705–2004) in Northern Vietnam. This chronology shows significant correlations with precipitation, temperature and PDSI (Sano et al., 2012).
The next record (1347–2013 AD) was published by Buckley et al. in 2017 and obtained from 71 cores of 37 trees from Quang Nam Province in central Vietnam. With this chronology, the Standardized Precipitation Evapotranspiration Index (SPEI) was reconstructed as an improvement of PDSI as a drought metric (Buckley et al., 2017).
In the last publication about *Fokienia hodginsii*, Buckley et al. (2019) present two new chronologies. The PMFH chronology (1555–2010 AD) was obtained from trees of Pu Mat National Park (Northern Vietnam), while the KKFH chronology (1057–2013 AD) was obtained from trees grown in the Kon Tum area (Central Vietnam). Along with previous *Fokienia hodginsii* chronologies, these new records were used to reconstruct the IPO (Buckley et al., 2019).

In addition to these studies conducted on Vietnamese trees, a chronology of *Fokienia hodginsii* growing on the northern Yunnan–Guizhou Plateau (southern China) has also been published (Su et al., 2017).

In 2018, Buckley et al. published an analysis of blue intensity records of annual rings of their QNFH core collection. Blue intensity is an image analysis–based measurement and was used as an indirect proxy measurement of wood density (Buckley et al., 2018).

Figure 5 and Table 1 summarize the details of the tree ring chronologies of *Fokienia hodginsii* published so far.

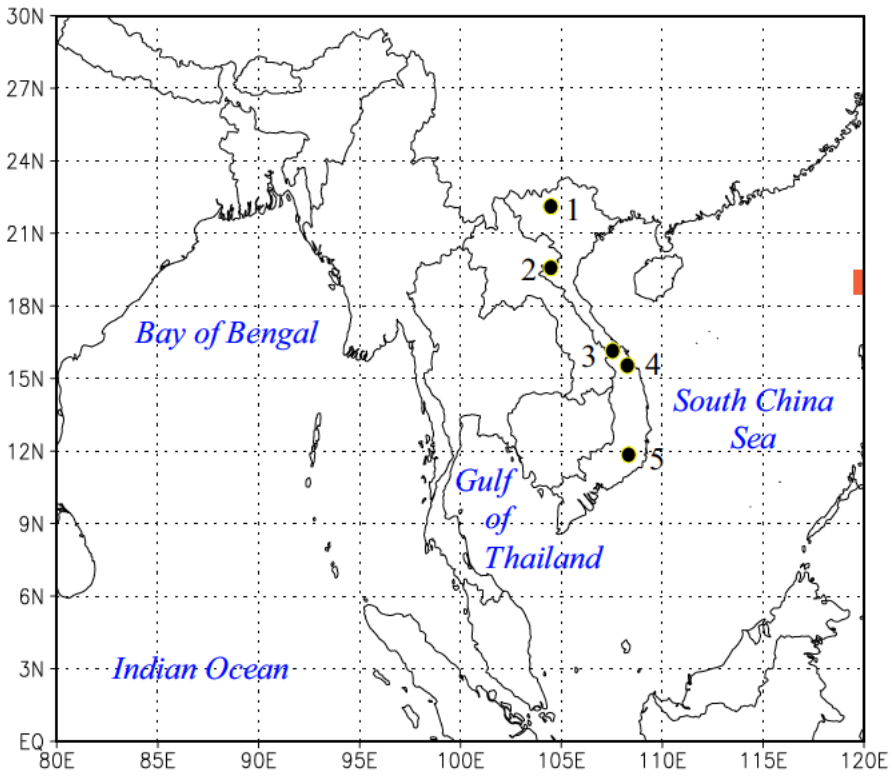

Figure 5: Sampling sites of the Fokienia hodginsii *chronologies published by Buckley. 1 = MCFH, 2 = PMFH, 3 = QNFH, 4 = KKFH and 5 = BDFH (Buckley et al., 2019).*

Table 1: Summary of all published Fokienia hodginsii *chronologies.*

Study	Site	Name	Period	Years	Mean series intercorrelation
Sano et al., 2009	Northern Vietnam	MCFH	1470–2004 AD	535	0.474
Buckley et al., 2010	Southern Vietnam	BDFH	1030–2008 AD	979	0.578
Sano et al., 2012	Northern Vietnam	-	1705–2004 AD	300	-
Buckley et al., 2017	Central Vietnam	QNFH	1347–2013 AD	667	0.526
Su et al., 2017	Southern China	-	1887–1996 AD	109	-
Buckley et al., 2019	Northern Vietnam	PMFH	1555–2010 AD	456	0.501
Buckley et al., 2019	Central Vietnam	KKFH	1057–2013 AD	957	0.576

The mean series intercorrelation (MSI) is a measure of the strength of the common signal in the chronology, which is typically the climate signal (*International Tree-Ring Data Bank Correlation Statistics*, n.d.).
The MSI of the *Fokienia hodginsii* chronologies varies between 0.474 and 0.578. These values are quite low but still reliable: the maximum value that the MSI can reach is about 0.900 (in species that react very clearly to climate), but a chronology may be still reliable with an MSI of 0.400. The average values are between 0.550 and 0.750. The MSI varies by species and region (*International Tree-Ring Data Bank Correlation Statistics*, n.d.).

Research questions

My master thesis will explore the potential of wood anatomy in the reconstruction of past climatic patterns in the Vietnamese conifer *Fokienia hodginsii*. This aim will be achieved by conducting a qualitative and quantitative analysis of the anatomical structure of *Fokienia hodginsii* cores and analysing the results in relation to climate data. The thesis therefore addresses a dendroclimatic issue in the context of a region particularly vulnerable to climate change, and it is a contribution to finding the missing link between climate and wood anatomy response in tropical regions. In fact, this is one of the first attempts to use wood anatomy in Southeast Asia, a region where few dendroclimatic studies have been previously carried out due to the tropical climate.

This master thesis is organized into the following chapters. Firstly, an introduction to *Fokienia hodginsii*, the previous studies done on that tree species, the Vietnamese climate and the sampling sites is presented. Secondly, the methods used are explained. Thirdly, the results are presented and, finally, they are discussed. In particular, the following questions are answered:

- What are the main anatomical characteristics of *Fokienia hodginsii*?
- What impact does climate have on the wood anatomical characteristics of Vietnamese *Fokienia hodginsii*?
- Can wood anatomical characteristics be used as better proxies than ring width?

This thesis is the result of a collaboration between the Swiss Federal Institute for Forest, Snow and Landscape Research WSL (represented by Prof. Dr. Paolo Cherubini), the Lamont–Doherty Earth Observatory (LDEO) of Columbia University in New York (represented by Dr. Brendan Buckley) and the University of Zurich (represented by Prof. Dr. Markus Egli).

Materials and methods

As highlighted in the paper of Von Arx et al. (2016), the challenge of quantitative wood anatomy is the need for high-quality and high-resolution images obtained from properly collected, stored and prepared samples. Each phase of the field and laboratory work can cause and produce considerable errors: only by working methodologically is it possible to minimize those errors (Von Arx et al., 2016). For this reason, a great part of the work of this thesis has been spent on the preparation of the samples. Different methods for the preparation of the samples for the anatomical analysis were tested in order to obtain the best-quality microslides.

Sampling

Dr Brendan Buckley sent 20 5-mm cores (Table 10), sampled in 2013, to the Swiss Federal Institute for Forest, Snow and Landscape Research WSL to perform anatomical analysis. These cores are part of the QNFH core collection, on which two papers have been published (Buckley et al., 2017, 2018). The tree rings of these cores have therefore already been cross dated and analysed with blue intensity.

The QNFH sample site is located in Central Vietnam, in the Tay Giang Protection Forest in the mountains of Quang Nam Province. The sample site is near the Laos border, at coordinates 15°09’ N, 107°41' E and at an elevation of 1,350 masl (Figure 5, point 3).

The forest with the trees from which the cores are extracted is classified as a mixed evergreen broadleaved-coniferous forest. The angiosperm species that coexist with *Fokienia hodginsii* in this type of forest are listed in Table 2. Most of the other gymnosperms growing in the QNFH forest belong to the Southern Hemisphere conifer family Podocarpaceae (Buckley et al., 2017).

Table 2: Common angiosperm species that coexist with Fokienia hodginsii *at the study site QNFH (Buckley et al., 2017). ‘Spp.’ means several species.*

Factor	Family	Genus	Species
Canopy dominant	Fagaceae	*Castanopsis*	spp.
		Lithocarpus	spp.
		Quercus	spp.
	Lauraceae	*Cinnamomum*	spp.
		Litsea	spp.
	Magnoliaceae	*Magnolia*	spp.
	Theaceae	*Anneslea*	*fragrans*
		Polyspora	spp.
		Schima	*wallichii*
Below canopy	Annonaceae	Polyalthia	spp.
	Asparagaceae	*Dracaena*	spp.
	Euphorbiaceae	Multiple	Multiple
	Melastomataceae	*Melastoma*	spp.
		Sonerila	spp.
	Lauraceae	*Cinnamomum*	spp.
		Litsea	spp.
	Moraceae	*Ficus*	spp.
	Primulaceae	*Ardisia*	spp.
	Rubiaceae	Ixora	spp.
		Lasianthus	spp.
	Rutaceae	*Clausena*	spp.
		Glycomis	spp.
Herbaceous layer	Araceae	*Arisaema*	sp.
	Asparagaceae	*Peliosanthes*	cf. *teta*
	Balsaminaceae	*Impatiens*	sp.
	Cyperaceae	*Cyperus*	*leucocephalus*
	Orchidaceae	Multiple	Multiple
	Piperaceae	*Piper*	spp.
	Poaceae	Bambusa	cf. *balcooa*
		Panicum	*notatum*
	Xanthorrhoeaceae	*Dianella*	*ensifolia*
	Zingiberaceae	*Amomum*	spp.
		Globba	spp.
		Zingiber	spp.

During a field trip in January 2020, additional samples were taken. The trip was organized with two purposes: to participate in the Southeast Asian Paleo Environments Consortium 2020 workshop (SAPEC-2020) and to collect new samples.

The topic of this week-long workshop organized by Dr Brendan Buckley was 'Data and Methods in the Paleo Proxy Sciences'. The participants were both experienced and young scientists from various parts of the world and specialized in several different fields: dendrosciences, sediments and corals, climate dynamics, hydrology, geology, ecology, archaeology and forestry. This workshop was an important opportunity for exchange and discussion among the participants. In the program, in addition to numerous lectures given both by the organizers and by the participants, there were also two days of sampling in the forest. Samples of different types and for different purposes were collected, including cores of *Fokienia hodginsii* for dendro analysis in this research and future studies.

The sampling area is located in Bidoup Nui Ba National Park in Southern Vietnam (Figure 5, point 5). In the same area, the cores of the collection BDFH analysed in the paper of Buckley et al., (2010) were sampled.

Figure 6: Sampling Fokienia hodginsii *in Bidoup Nui Ba National Park, 7 January 2020.*

In dendrochronological studies, the search and selection of the sampling site and the tree to sample comprise a fundamental part of the research because the location of the site directly influences the research questions and results. In order to ensure statistical value, it is necessary to provide for replicates within the same sampling site so that all the samples of a site have similar signals (Schweingruber et al., 1990). According to Schweingruber et al. (1990), two basic principles should be considered when planning the sampling strategy: site homogeneity largely determines the quality of the chronology, and stand development affects cambial

activity. The first principle aims to reduce variability due to climatic and environmental variability, and the second aims to reduce variability caused by tree competition (Schweingruber et al., 1990).

Since *Fokienia hodginsii* is a rare tree species in Vietnam, the sampling strategy was simply to core the few trees that were present in the sampling area. Because of Mr. Le Canh Nam's excellent knowledge of the forest, it was possible to find and identify nine trees in two areas of approximately 1 km^2 each, located 4.8 km apart from each other. The 16 samples (Table 14) were taken with a 5-mm increment borer, as were the samples received from Dr Brendan Buckley. When extracting the bore cores, attention was paid to drive the corer towards the pith in an exact radial direction. In addition to the corer, a breast-height wooden support was used to apply sufficient pressure at the beginning of the coring without compromising the quality of the sample. This is particularly important if wood anatomical analysis is planned. Every core extracted was immediately marked with a pencil with the corresponding sample name. Next, each sample was placed in a paper straw and then in a plastic tube. In the following days, the samples were placed under a weight so as to dry without bending.

The diameters at breast height of the trees were between 40 and 65 cm. The sampling site is a mixed evergreen broadleaved-coniferous forest growing on a thick humus horizon with a slope between 5° and 25°. Although the forest is located on the side of the main road connecting the cities of Dalat and Nha Trang, there are not many signs of humans except for garbage in the strip of forest very close to the road. The sampling site is located within Bidoup Nui Ba National Park, whose forest protection measures have certainly contributed to limiting human disturbance (such as logging) in the forest. The Vietnam War did not destroy or particularly affect this forest. The presence of rare and long-living trees such as *Fokienia hodginsii* is evidence that human disturbance is limited.

Sample preparation

All the 20 cores received from the Tree Ring Lab of the Lamont-Doherty Earth Observatory were sanded and glued on wooden mounts. In order to proceed with the preparation of the microsections, the cores had to be detached from their supports. The cores glued to the mounts were left immersed in hot water for about an hour; then, with the help of an awl and cutter, they were detached and placed in a wooden box for cores so that they dried without bending. Before the cores were stored, the glue residue had to be thoroughly rinsed out.

Wood anatomical laboratory work

To obtain the best microsections, several methods were tested. The first method tested was embedding the samples into the paraffin and cutting the microsections with the rotatory microtome. This method was applied to 10 cores.

The samples were cut obliquely (so that several tree rings were on two different pieces) into pieces about three centimetres long, then placed in special plastic boxes. These little boxes are made like a grid: they keep the sample inside but let liquid solutions into the sample. The name of the sample was written in pencil on each box. All samples, each in its own box, were bathed for 24 h in alcohol (to dehydrate) and in paraffine. This process, which occurs automatically in a specific machine, was meant to ensure that paraffin got into each cell. Without ever dropping out below the melting point of paraffine, the samples were placed in paraffin blocks. In this step, it was important that the samples were oriented correctly (i.e., with the direction of the fibres oriented perpendicularly to the paraffin surface). After this step, the samples were quickly solidified on a cold plate.

Before cutting the samples with the microtome, it was necessary to remove the excess paraffin with a cutter and then pre-cut the surface with the microtome in order to make it perfectly smooth. Finally, the microsections were cut to a thickness of 12 µm. As soon as they were cut, they were put in tepid water (37°C) to prevent the paraffine from rolling over and to make the sample well stretched. From the water, the microsections were then transferred to a glass slide previously wetted with Eiweiss glycerin, which ensured that the sample remained glued to the slide. The samples then stayed in the oven at 60°C for about two hours before being stained. The high temperature caused some of the paraffin to dissolve; the rest was chemically removed before staining.

Embedding the samples in paraffin should have prevented damage to the cell structure (Von Arx et al., 2016). However, this method did not produce the expected results: most of the cell walls were broken or damaged. As a result, the image quality that could have been obtained from these microsections was not sufficient to perform the analysis.

There are alternative methods to the use of paraffin to prevent cell walls from breaking, such as using a solution of starch and water or soaking (or boiling) the samples in water (Von Arx et al., 2016). The second method used in this study was cutting the samples with a laboratory sledge microtome. Corn starch was mixed with water until a non-Newtonian solution was obtained. This solution was then applied with a brush directly to the samples (either untreated or embedded paraffin samples). The sample was then cut to a thickness of about 15 µm with the main blade holder positioned at an angle of 50° away from the sample. At the end of the cutting process, the starch was washed away with water. The microsection was then transferred onto a slide with the help of a fine brush and a needle and covered with few drops of glycerol to

prevent it from drying out. The quality of microsections not embedded in paraffin was directly checked under the microscope.

Figure 7: The rotary microtome during the pre-cutting phase (left) and pre-cut samples embedded in paraffin (right).

In both types of microtomes, it is necessary to move and change the blades frequently to prevent them from being damaged and leaving marks of microsection. Another very important aspect to consider when using both types of microtomes is the cutting direction. The QNFH samples were not always sanded in the correct direction, but to avoid under- or over-estimating the anatomical parameters, it was necessary that the microsections were cut perfectly perpendicular to the direction of the tracheids.

The samples embedded in paraffin and glued to the slides using albumin (Eiweiss glycerin) were stained in series by being sorted into baskets of 10 slides, which were soaked in xylol (twice for 15 minutes), then in ethanol (twice for 15 minutes) and in stain (once for 15 minutes). Xylol is a solvent that helps to remove remaining paraffin and is a toxic substance. The stain was a 1:1 mixture of safranine and Astra blue. The first stained the lignified parts of the samples red; the second stained the non-lignified parts blue. The samples were then quickly soaked once in water and twice in ethanol to dehydrate them. During this process, all the excess stain was removed. Finally, the samples were removed one at a time from the basket, carefully dried with a piece of absorbent paper and covered with two drops of Euparal (a mounting medium) and then with the coverglass. The slides were placed on a metal plate covered with paper and held with two magnets in order to increase the pressure. In this setting, they remained for at least 48 h at room temperature (or for 12 h at 60°C in the oven), so that the Euparal became hard and kept each slide, sample and coverglass glued together. At the end of this procedure, the permanent slides were ready. Before analysing them under the microscope or scanning them, they were cleaned with a cutter blade to remove any excess Euparal.

Microsections that had been placed on slides and covered with glycerol were stained one at a time using pipettes and not left soaking in solutions. The steps were similar, but xylol was not used if the samples were not embedded in paraffin. The glycerol was rinsed with water, then a few drops of stain were left on the sample for about four minutes. Next, the excess was rinsed off with water, a 75% alcohol solution and a 96% alcohol solution. Finally, the samples were gently dried with a piece of absorbent paper and sealed with Euparal, as described above.

Wood anatomical analysis

Before the microslides were digitized, their quality was checked with the microscope at different magnifications. This allowed a selection to be made between good-quality and bad-quality microslides. Of the many microslides prepared, only a small number were selected. The selected microslides were all from one of the five cores listed in Table 3; however, not all of the tree rings of those cores were analysed due to the difficulty of creating microslides of excellent quality. To avoid time-consuming manual editing and the production of erroneous data while analysing the scans with image-analysis software, only perfectly prepared samples were scanned. Figure 8 shows the sample depth.

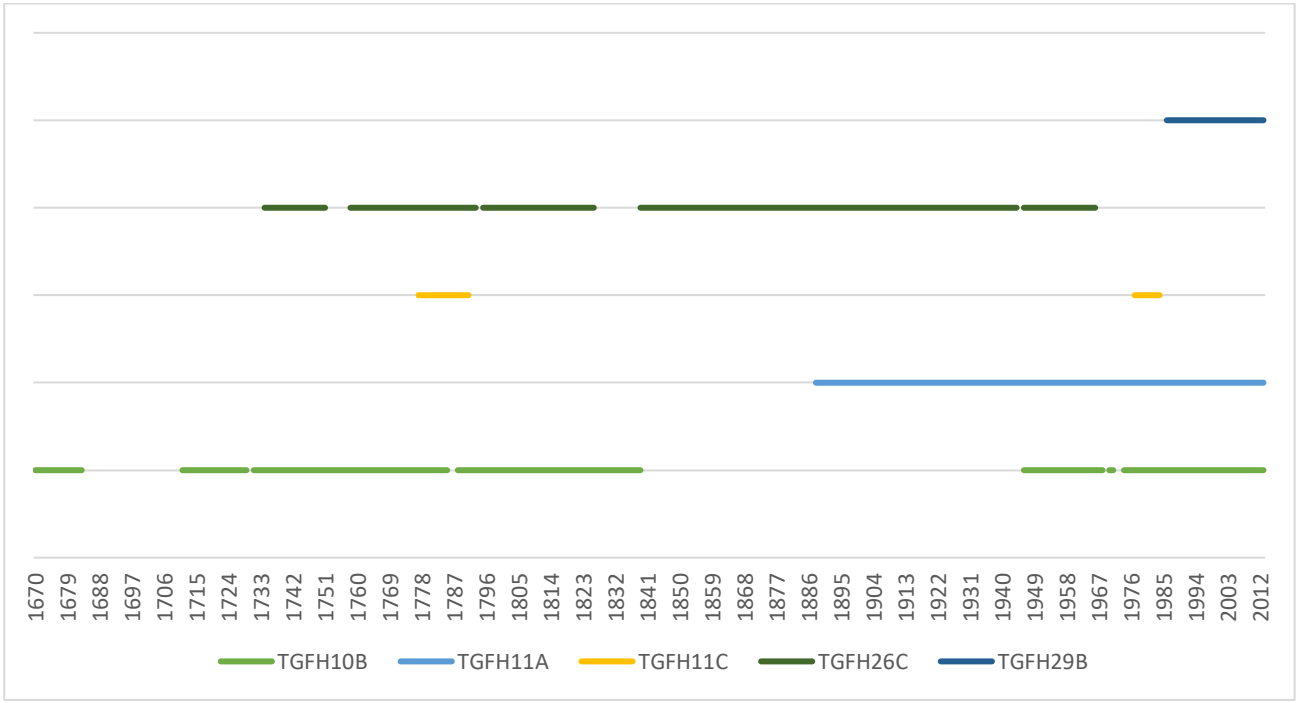

Figure 8: Sample depth for anatomical analysis.

Table 3: Cores of the QNFH collection used for anatomical analysis.

Tree name	Sample	First ring	Last ring	Number of annual rings
TGFH10	B	1550	2013	463
TGFH11	A	1600	2013	413
	C	1670	2013	343
TGFH26	C	1720	1995	275
TGFH29	B	1573	2013	440

The microslides were subsequently scanned with a ZEISS Axio Scan. The images produced by the scanner were very large files: to be transferred, they were compressed into BigTIFF format, cropped with Adobe Photoshop (removing the empty space to reduce the size of the file) and saved in an uncompressed TIFF format.

There are several image-analysis software programs used in the field of quantitative wood anatomy. Von Arx et al. (2016) present an overview of the most commonly used programs, dividing them into two groups: general tools and specialized tools. Among the general tools, there are software programs such as ImageJ, CellProfiler, Image-Pro Plus, NIS-Elements and AxioVision (Von Arx et al., 2016). The two specialized programs cited by Von Arx et al. (2016) are ROXAS and WinCELL. The main differences between these two tools are that ROXAS works with vectorized object models and WinCELL with pixeled object models and that in ROXAS, the tree ring analysis is computed automatically (Von Arx et al., 2016).
For this research project, WinCELL 2020a was used. This software allowed to open the uncompressed TIFF files, manually draw the tree rings and automatically analyse the anatomical features of each ring. After drawing the rings, it was very important to determine the direction in which the cells grew and therefore the direction in which the parameters of the cells had to be measured.
The software allows to manually set up the cell recognition filter so that artefacts, intercellular spaces or other objects are not counted as cells. In the case of *Fokienia hodginsii*, five filter variables were added to the original settings:

- Area < 100 μm^2: This setting allows one to exclude background noise (due to image colour differences) and intercellular spaces. This value is a compromise that allows for the inclusion of very small cells that are present in latewood and, at the same time, the exclusion of very small objects that are not cells.
- Length/Width < 0.15: The main aim of this setting is to prevent rays from being counted as tracheid cells.
- Length > 200 µm: As in the previous setting, the main aim of this setting is to prevent rays from being counted as tracheid cells.

- Width > 170 µm: This setting excludes possible artefacts, such as two cells that are recognized as one due to the damage of the cell wall between them.
- Length/Width > 4.5: As in the previous setting, the main aim of this setting is to avoid neighbouring cells being recognized as one.

The software produced a text document with a large amount of data. For each individual cell and ring, many parameters were measured (Table 4), illustrated in Figure 9. All the parameters listed in the table were automatically calculated for each ring by WinCELL, except for average cell length (ACL) and average wall thickness (AWT), which were two parameters calculated by WinCELL for each cell and then aggregated by averaging the values of all cells of one ring.

Table 4: Wood anatomical parameters.

Parameter	***Acronym***	***Unit of measurement***
Ring width	RW2	µm
Percent total lumen area	%LA	%
Average lumen area	ALA	μm^2
Average lumen width	ALW	µm
Average lumen length	ALL	µm
Average cell length	ACL	µm
Average lumen perimeter	ALP	µm
Average lumen form coefficient	AFC	(μm^2/ μm^2)
Average lumen length/width	ALLW	(µm/µm)
Average wall thickness	AWT	µm

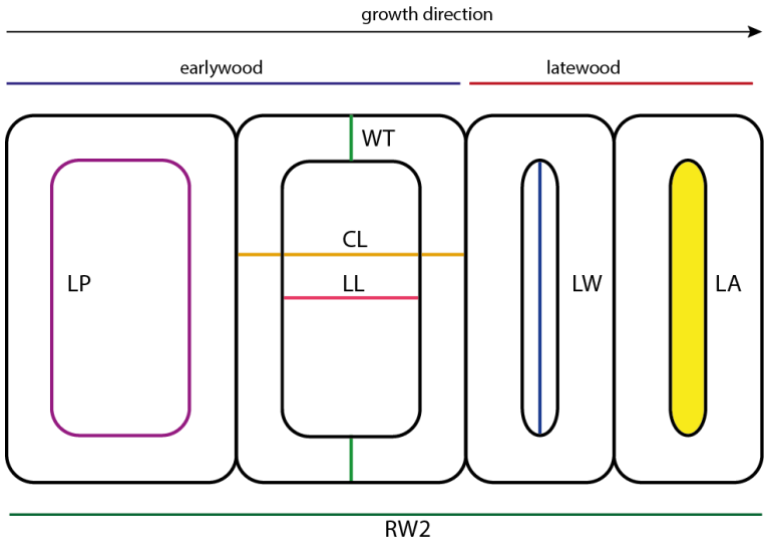

Figure 9: Wood anatomical parameters.

Statistical analysis

The KNMI Climate Explorer (https://climexp.knmi.nl; Trouet & Van Oldenborgh, 2013) was used to calculate the spatial correlations between the anatomical parameters and the climatic data. This web-based research tool allows one to upload time series (in this case, wood anatomical time series) and correlate them with other time series, either uploaded by the user or already present on the KNMI Climate Explorer. Numerous time series of global climatic data are already available on the website, which includes several options for analysing the data. Among them, there is the possibility to do correlations or regression analysis, to calculate correlation coefficients and to calculate lagged correlations. These kinds of comparisons can be made between two time series or between a time series and a gridded dataset. In the latter case, the result is a correlation, regression or composite map (Trouet & Van Oldenborgh, 2013).

In the context of this thesis, the KNMI Climate Explorer was used mainly to do this kind of spatial analysis, while R was used for the correlation between two time series. Analyses between wood anatomical data and climatic data were done both with monthly data (starting from the previous September's data) and with aggregated data for groups of three months each. The reference to months is made by indicating the initials of the months (for example: AMJ are the months of April, May and June). When discussing about the autumn months (September-December), it always refers to those of the previous year compared to the year in which the anatomical parameters were dated.

Maximum temperature

The maximum temperature data were downloaded from the KNMI Climate Explorer and are part of Version 4 of the Climatic Research Unit gridded Time Series dataset (CRU TS4.04), which also contains nine other climatic variables (Harris et al., 2020). This dataset is based on weather station observations from the period 1901–2018 and has a monthly temporal resolution and a spatial resolution of 0.5°. The CRU TS is widely used for calibrating paleoclimate reconstructions and analysing climatic variability as well for several other purposes (Harris et al., 2020).

Precipitation

Dr Brendan Buckley provided precipitation data measured at 11 climate stations in the region. These data were measured in mm with a temporal resolution of one month from 1980 to 2006. Mr. Le Canh Nam (from the Forest Science Institute of Central Highlands and South of Central Vietnam) identified the three stations closest to the sampling site. The data of these three stations were averaged.

Standardized Precipitation Evapotranspiration Index

In the context of this study, it is interesting to relate a drought index to dendroclimatic data, as Central Vietnam's climate is characterized by a rainy season and a drier period. The Standardized Precipitation

Evapotranspiration Index (SPEI) is a drought index that allows one to discriminate between different drought types and impacts (Beguería et al., 2014). It was developed in 2010 and is suitable for studies on climate change because it includes temperature (unlike the Standardized Precipitation Index) as a factor affecting drought and is multiscalar (unlike the Palmer Drought Severity Index), a feature that allows one to assess drought in relation to different hydrological systems and differentiate among different drought types (Beguería et al., 2014).

The SPEI data were obtained from the Global SPEI database (https://spei.csic.es/database.html). These data were calculated from monthly evapotranspiration and precipitation data from the Climate Research Unit (University of Anglia, UK) dataset; the spatial resolution is 0.5°, and the temporal resolution is monthly (Buckley et al., 2017). The data describe the deviation of the water balance of the month from the long-term mean: negative values indicate droughts, and positive values indicate water surplus (*Drought Indices*, 2020).

Wood anatomical parameters

The first step of WinCELL's output processing was to assign a year to each analysed ring. This was possible because of the data provided by Dr Brendan Buckley, which shows the width of each ring and the year that was assigned to each ring by cross dating. The samples analysed in WinCELL are segments about three centimetres long, cut from the original core. To identify each ring's corresponding year, it was necessary to correlate the series of ring widths (10–70 rings) measured in WinCELL with the series of ring widths of the entire core (300–500 rings). The correlation was made using R. In some samples, it was necessary to add missing rings to optimize the correlation.

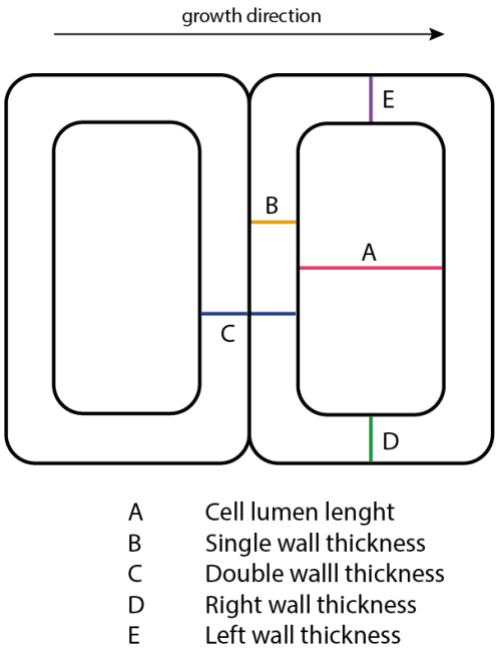

Figure 10: Parameters to define LW (adapted from Denne, 1988.)

Earlywood (EW) and latewood (LW) cells were distinguished according to the definition of LW proposed by Mork in 1928. The definition says that '*zum Herstholz sind alle jene Tracheiden zu rechnen, deren gemeinsame Zellwande zwischen zwei Zellenhohlraumen multipliziert mit 2 = oder > als das Zellenvolumen sind; zum Friihjahrsholz alle die Zellen, in denen der Zellenhohlraum > als die gemeinsame Zellwand multipliziert mit 2 (alles in radialer Richtung gemessen) ist, oder kurz: Herbstholz: Gemeinsame Zellwand x 2 > Zellenhohlraum. Friihjahrsholz: Zellenhohlraum > gemeinsame Zellwand x 2*' (Denne, 1988, p. 59). This definition may be interpreted in different ways: some authors have interpreted that the definition of LW is 2B ≥ A and others that it is 2C ≥ A (Figure 10).

Denne (1988) has shown that the difference between the percentage of LW resulting from the two interpretations is species specific: for some species, the difference is small; for others, larger; and for some species, neither of the two definitions is suitable (neither of them distinguishes EW from LW). Mork's definition should therefore not be taken as a standard but rather as a basis for differentiation between EW and LW (Denne, 1988).

To find the best definition of LW in *Fokienia hodginsii*, several formulas were tested. The sum of the cell wall thicknesses on the right (D in Figure 10) and left (E in Figure 10) was used as a cell wall parameter. These parameters were read in the WinCELL output. The sum of the cell walls was multiplied by several factors between 1 and 3 and compared with the length of the lumen; applying the formula on the LW cells closest to the EW cells (i.e., the LW cells with the longest lumens) and visually observing the distribution of EW and LW cells in R (Figure 11), 2(D+E) ≥ A was determined to be the best method for finding the definition of LW for *Fokienia hodginsii*.

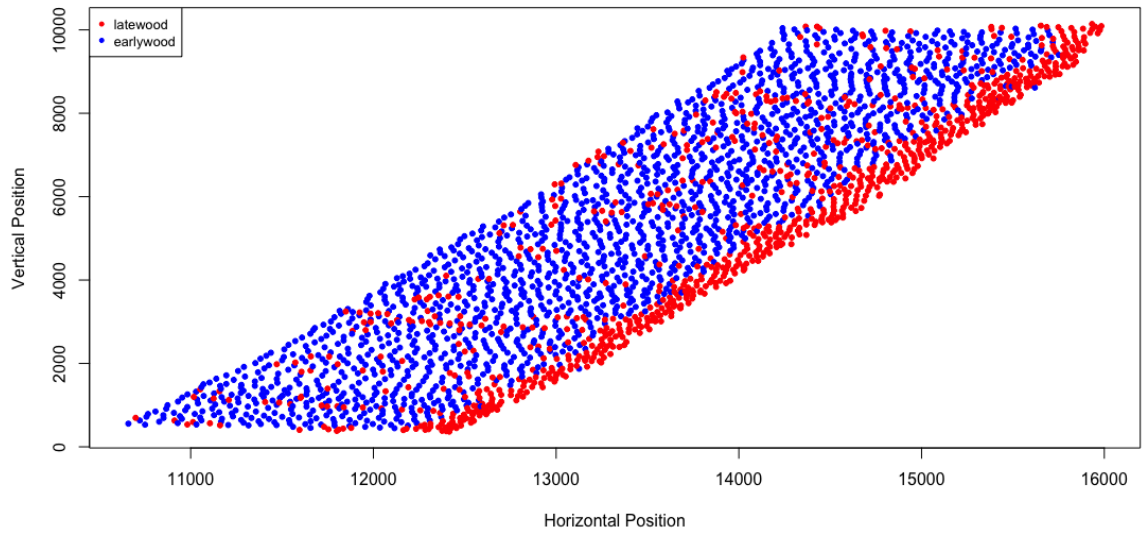

Figure 11: EW and LW differentiation (sample TGFH10B, the year 1962).

Because of this method, all cells measured with WinCELL were divided into the categories of EW and LW cells. The parameters of Table 4 were calculated only for EW and LW cells; to differentiate them, the letter 'e' or 'l' was added in front of the parameter abbreviation. For example, ALA is the average lumen area of all the cells of a ring, eALA the average lumen area of the EW cells of a ring and lALA the average lumen area of the LW cells of a ring.

All series of anatomical parameters were then detrended. The need to detrend anatomical parameter series is discussed in the literature: for example, Bryukhanova and Fonti (2013) and Lehejček et al. (2017) have detrended wood anatomical parameters series; on the contrary, Ziaco et al. (2016) and Liang et al. (2013) have not. In the case of this research, the series have been detrended mainly to remove differences in series

amplitude and to remove any possible trends. A 30-year spline was applied using the R package dplR on each series of anatomical parameters. This is a high-frequency detrending that retains the short-term variations of the series (Figure 12). The resulting value is dimensionless, as the data have been divided by the smoothed value. For this reason, all the detrended indices vary around 1.

Finally, the average of the detrended data of each parameter for each year was calculated. In this way, one chronology of data was obtained for each parameter.

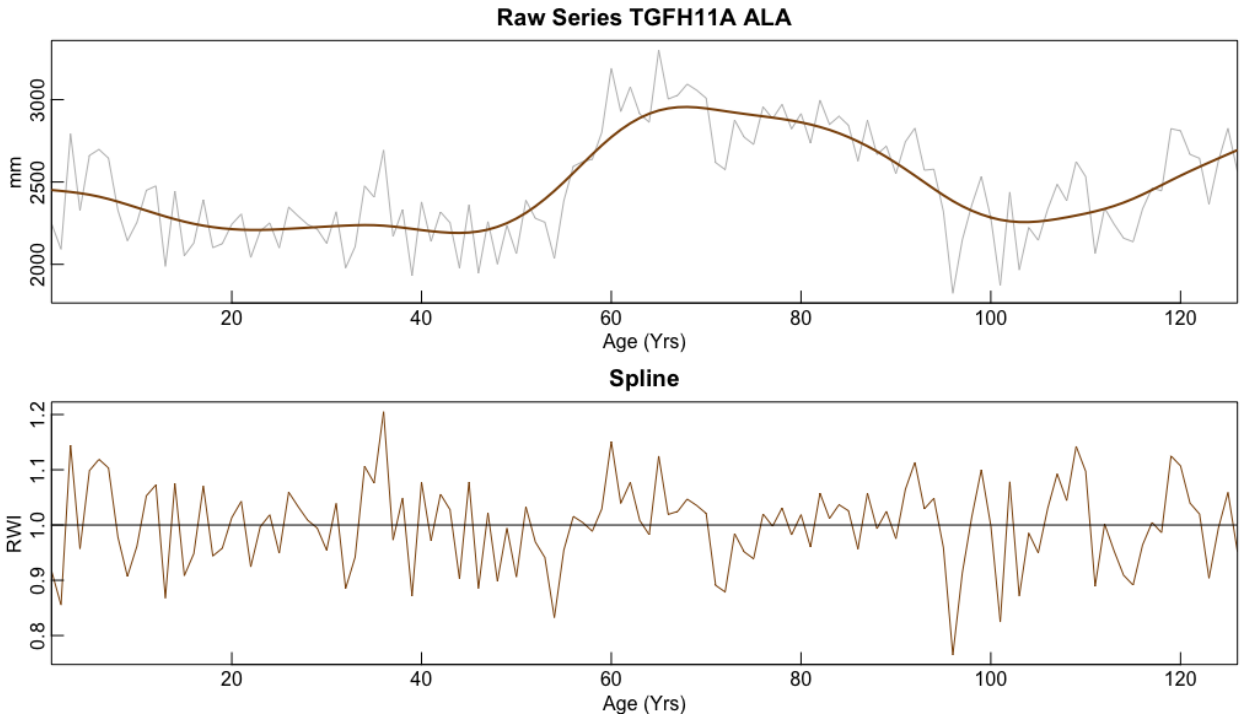

Figure 12: Detrending with a 30-year spline of the ALA series of the sample TGFH11A.
The units of measurement on the Y-axis are wrong: in the plot above, the unit is µm², while in the plot below, it is a dimensionless ALA index. R automatically produces the plots, assuming that they are ring width data.

Blue intensity data

In addition to the ring width data for the QNFH samples, Dr Brendan Buckley also provided the blue intensity (BI) measurement data of the paper (Buckley et al., 2018). Blue intensity is an image analysis–based measure of the absorbency of blue light by wood. Since lignin is more likely to absorb blue light and cellulose and hemicellulose are less likely, BI is high (i.e., there is a higher degree of reflected blue light) when the wood is less dense (i.e., less lignified; Buckley et al., 2018).

The BI data received contained three different datasets, each expressed for each tree ring of the 29 core samples analysed in the study, among which are also the samples analysed anatomically in this thesis.

The three datasets are earlywood BI (EWBI), latewood BI (LWBI) and ΔBI, which is the difference between EWBI and LWBI. This last parameter was calculated in order to reduce the effects of colour changes at the heartwood–sapwood boundary. EWBI represents the minimum density of the EW and LWBI the maximum

density of the LW: to calculate these values, the highest 85% of the BI values in the EW area and the lowest 15% of the BI values in the LW area (Figure 13) were selected, respectively (Buckley et al., 2018).

Dr Brendan Buckley provided the original measurements (Buckley et al., 2018), which were detrended in the research. In the context of this thesis, the data were detrended with a 30-year spline (the same method used for the wood anatomical time series) before being correlated in R with the anatomical parameters.

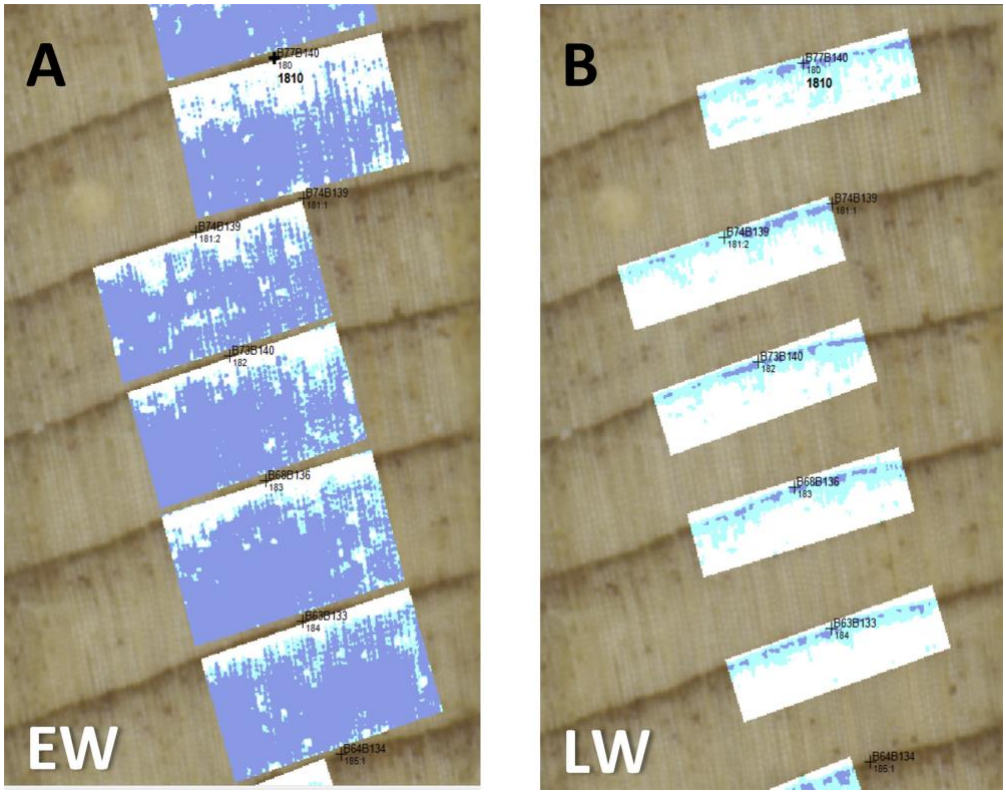

Figure 13: BI measurement in CooRecorder. Highlighted in dark blue are 85% of the least lignified pixels in the earlywood EW and 15% of the most lignified pixels in the LW, respectively (Buckley et al., 2018).

Results

Wood anatomical characterization of *Fokienia hodginsii*

The structure of the rings in the transversal section is simple: every tree ring is composed of many rows of earlywood (EW) cells and by few rows of latewood (LW) cells. However, every cell is unique, and there are great variations in cell and lumen dimensions, wall thicknesses and other structural features.

The ring boundaries are usually distinct; however, in some samples, detection of the ring border is not intuitive because the LW is very thin. The transition from EW to LW within the same tree ring is abrupt in most of the samples. EW tracheids are more than twice as long on average and have an area three times as large (Figure 15). However, there is great variability between samples, as in the right-side image of Figure 14, where EW and LW cells are not always distinguishable. Because of the distinct boundaries and the abrupt transition from EW to LW, tree rings are clearly visible (if wide enough) even at a macroscopic level.

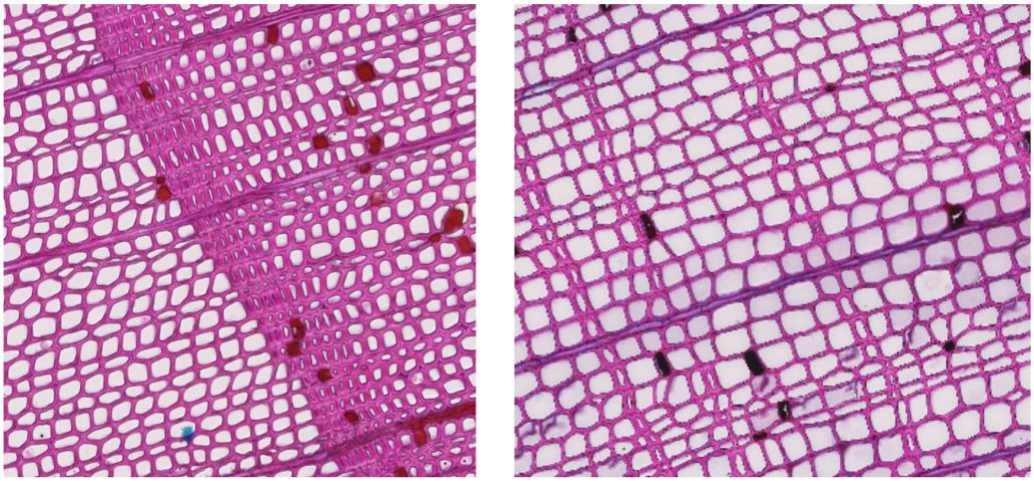

Figure 14: Distinct and indistinct ring boundaries.

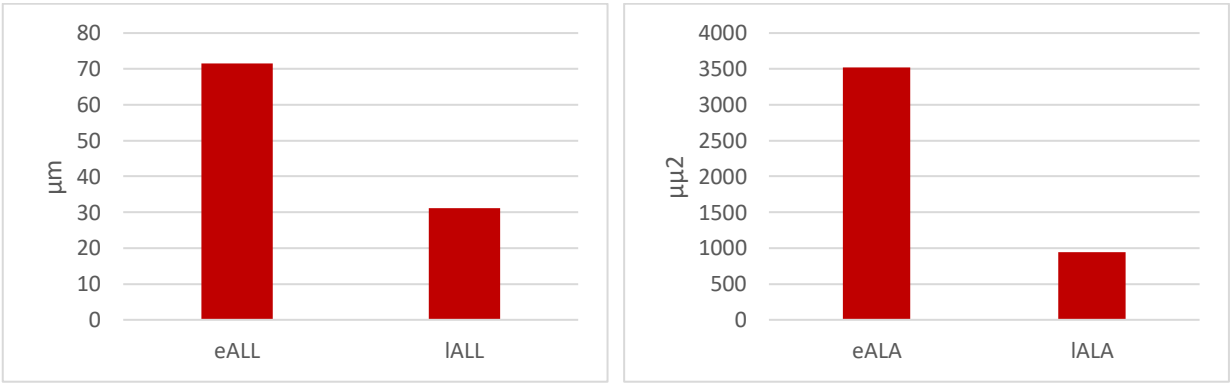

Figure 15: Difference between average lumen length (ALL, left) and average lumen area (ALA, right) in EW and LW, respectively.

There are no resin ducts, but the anatomical structure is characterized by many rays. Figure 14 shows that some cells are full of a dark substance. This feature will be discussed more deeply in the section 'Axial parenchyma'.

The radial section (Figure 16, left) shows that the tracheid pitting is mostly uniseriate and sometimes biseriate. There is no helical or callitroid thickening in tracheids. Ray tracheids are absent, and ray parenchyma end walls are smooth. The crossfields are cupressoid.

From the tangential section (Figure 16, right), it can be observed that rays are exclusively uniseriate and that the average ray height is low (up to five cells). At high magnification, the pits of the tracheids are visible.

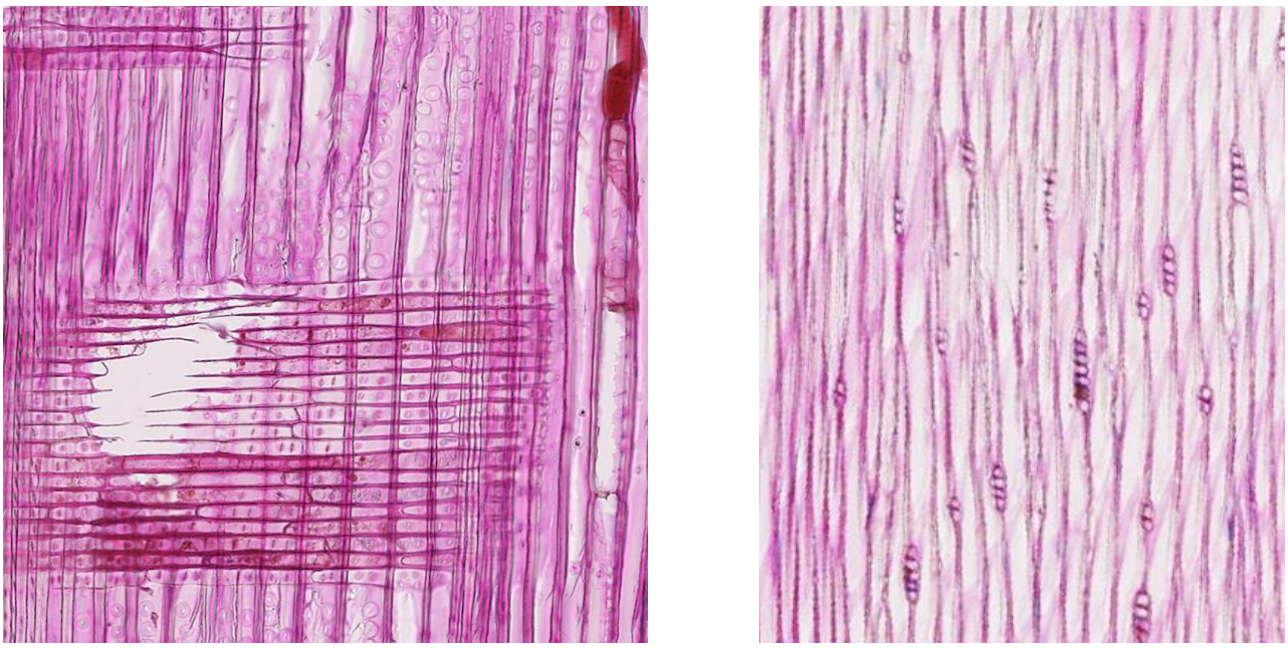

Figure 16: Crossfield in a radial section (left) and tangential section (right).

Axial parenchyma

Axial parenchyma are cells with support and storage functions and are widely present in *Fokienia hodginsii*. The arrangement of axial parenchyma is both diffuse and tangentially zonate. Tangentially zonate axial parenchyma is defined as 'parenchyma strands grouped into short or longer tangential (or oblique) lines more or less parallel to the growth ring boundaries, most frequent in the transition zone from earlywood to latewood or in latewood' (Baas, Pieter, et al., 2004, p. 37). In the samples analysed, axial parenchyma is widely present both in EW and in LW.

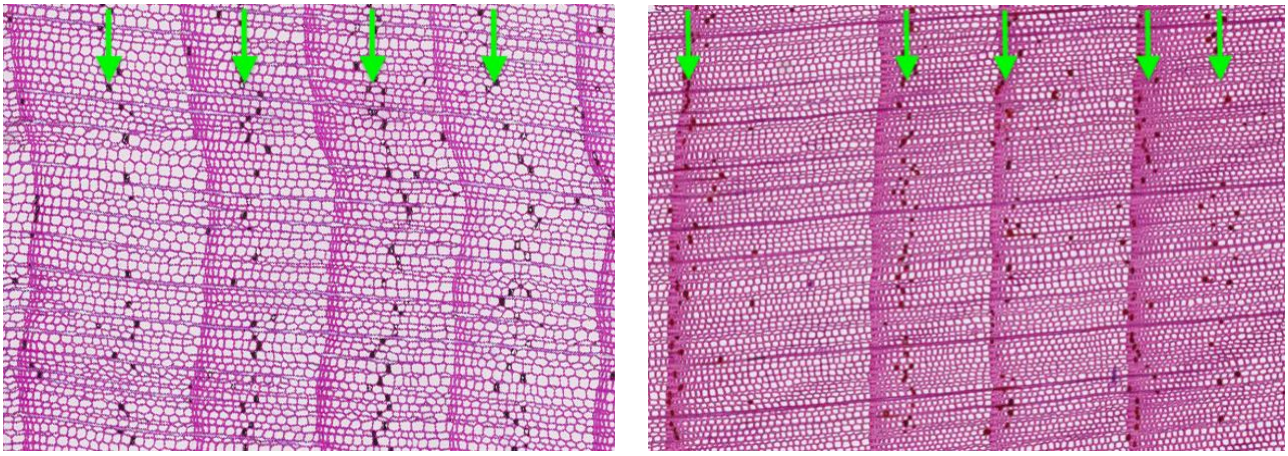

Figure 17: Tangentially zonate axial parenchyma bands are marked with green arrows.

As Baas, Pieter et al. (2004) wrote, the content of axial parenchyma may be removed during sample preparation. In this thesis, an influence of the preparation on the content of the axial parenchyma was noticed. The content is orange-brown in samples prepared with starch (Figure 17, right; Figure 18), while it was black and partly removed in samples embedded in paraffin and processed with xylol (Figure 17, left).

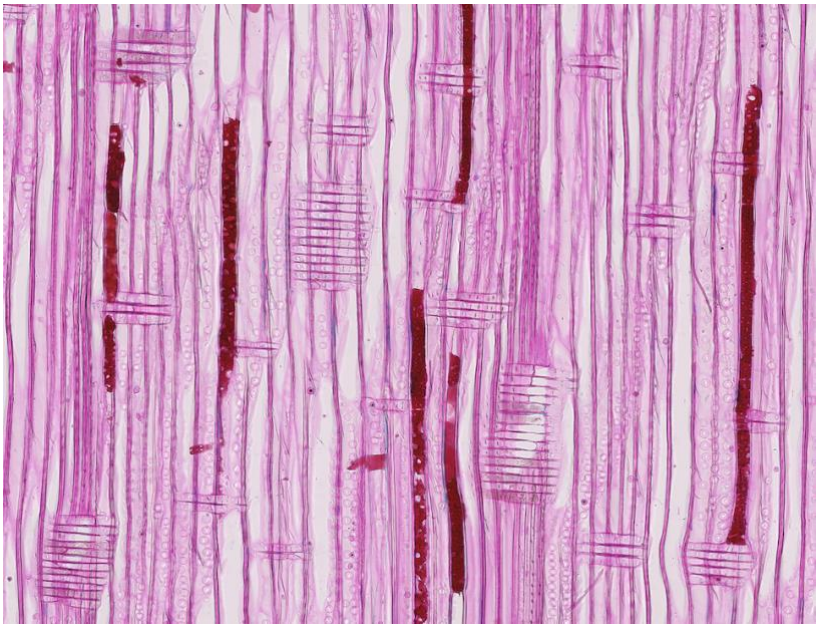

Figure 18: Axial parenchyma in a longitudinal section.

A visual analysis of five samples for the period 1946–2013 was carried out with the aim of understanding whether these axial parenchyma bands were present in the samples in the same years or present irregularly in the various samples. Figure 19 shows that the sample size analysed is of two or three samples for each year. In only six years, three out of three rings analysed had visible axial parenchyma bands. For most of the years, only one sample of the two or three analysed shows bands of axial parenchyma cells.

The analysis shows that in the period 1946–1980, the bands are mainly found in LW, while in the period 1981–2013, they are located mainly in EW.

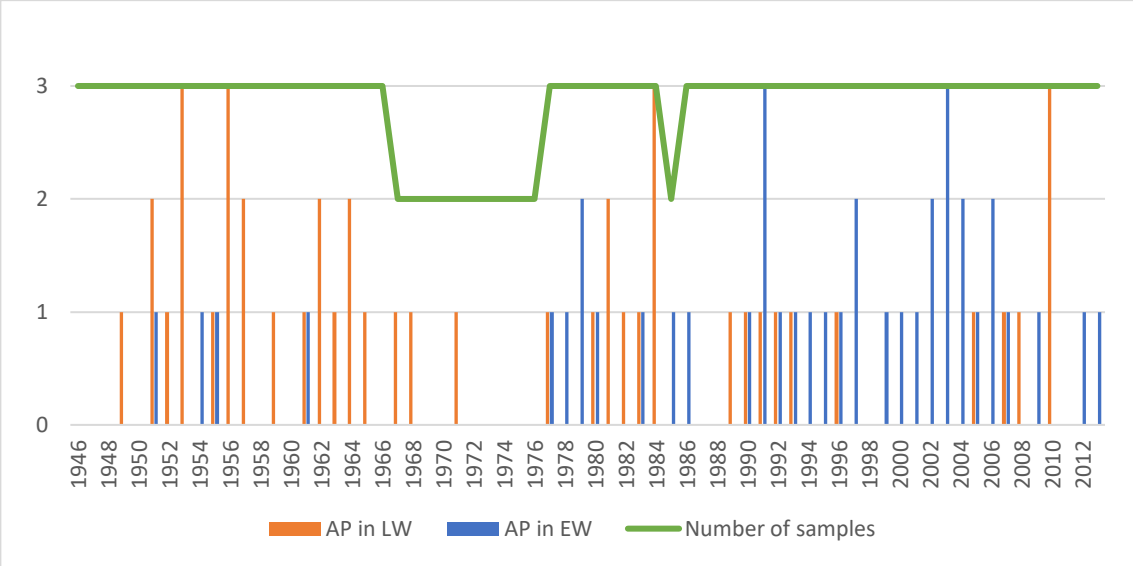

Figure 19: Presence of rows of filled axial parenchyma cells in EW or LW per year.

Dendrochronological and anatomical data

The ring width measurements made with WinCELL were compared with measurements made by Dr Brendan Buckley. The unit of measurement of both measurements should be micrometres; however, the data are different. The source of this error remains unclear. In any case, the correlation between the measurements made at the Lamont-Doherty Earth Observatory (LDEO) and those made at the Swiss Federal Institute for Forest, Snow and Landscape Research WSL is very good for most samples. For two samples, to improve the correlation, it was necessary to insert missing rings into the measurements made at the WSL. One of these was the TGFH10B1 sample, for which the best correlation without adding missing rings was just 0.3956 (R^2). When three missing rings were entered in the years 1969, 1972 and 1973, the correlation increased to 0.9133 (R^2, Figure 20). The 1969 ring is also missing in the measurements made at the LDEO.

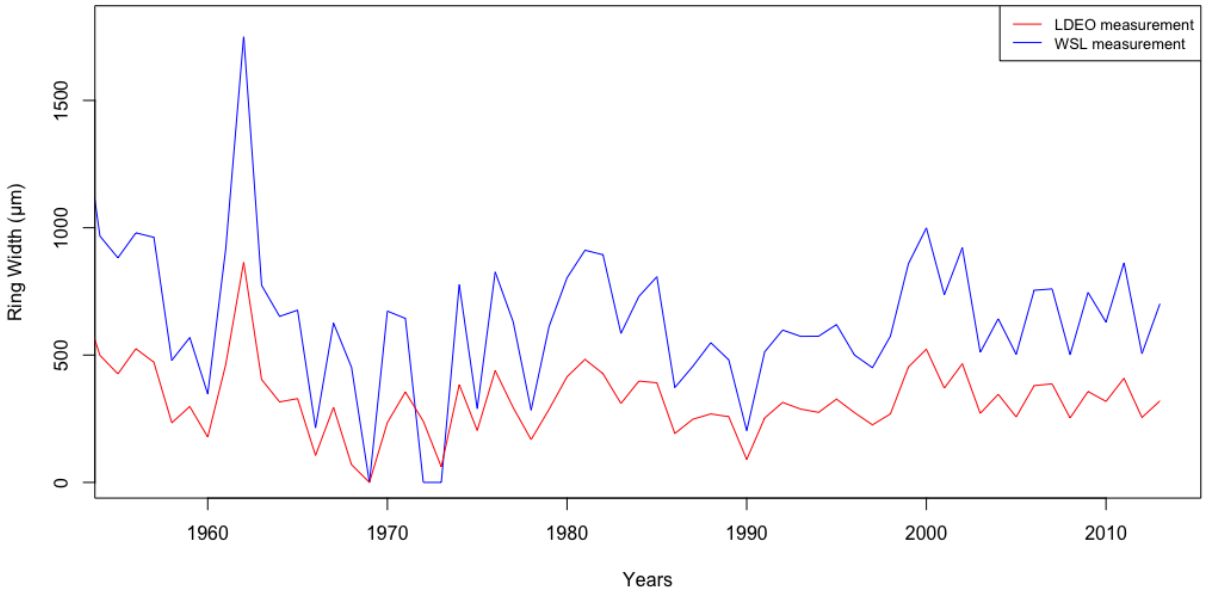

Figure 20: Comparison of the ring width measurements made at the LDEO (Columbia University, NY) and the WSL for the sample TGFH10B1. The R^2 value is 0.9133.

The comparison between the two detrended ring width chronologies (Figure 21) shows great similarity. Most of the differences are due to the sample size: for example, the data of the ring width measured at the WSL (RW2) of the year 1678 is based on only one sample, while the data of the ring width measured at the LDEO (RW1) is based on five. For the calculation in this thesis of the RW1 chronology, the complete data of five cores were used, while the RW2 chronology is based on the annual ring width of one to three cores. The data for the rings of the years 1684–1710 and the year 1730 are missing (Figure 8).

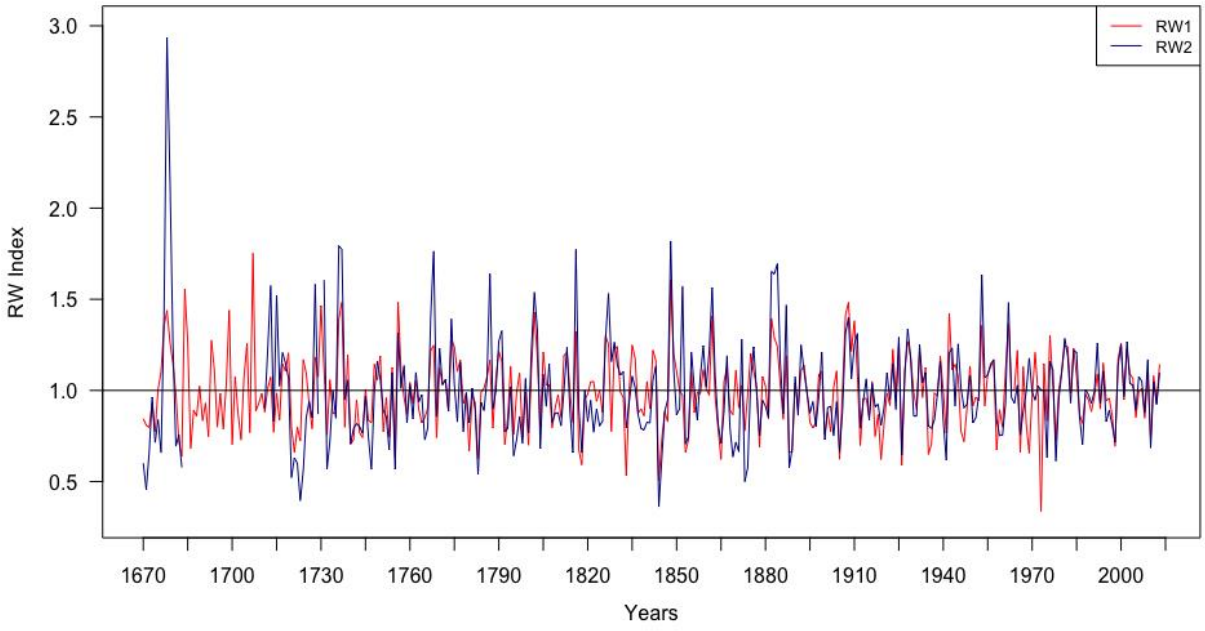

Figure 21: Comparison between the detrended tree ring width measured at the LDEO (RW1) and at the WSL (RW2).

Also, the anatomical chronologies range from 1670 to 2013, with missing data from 1684 to 1710 and in the year 1730. In Figure 22 are displayed the chronologies of ALA, eALA and lALA. The amplitude of lALA data is much greater than that of ALA, which in turn has a greater amplitude than eALA. The three parameters do not always follow a similar trend: in some years, for example, lALA is lower than the average, while eALA and ALA have high values.

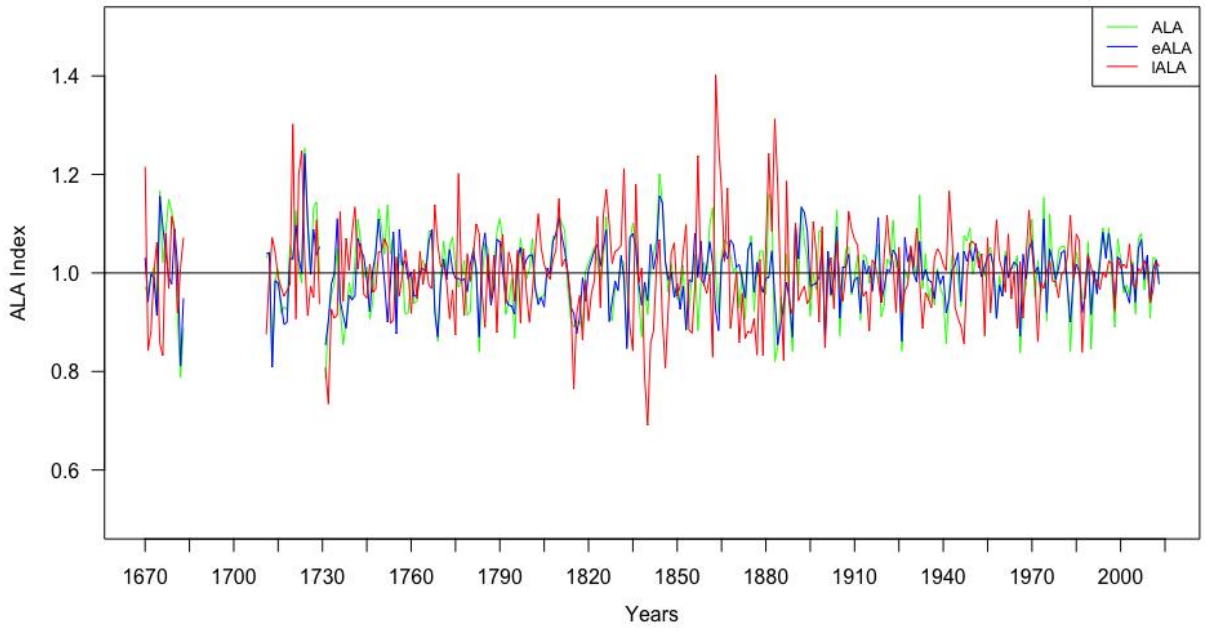

Figure 22: ALA, eALA and lALA chronologies.

When comparing the anatomical chronologies for the entire ring, high correlations ($r > 0.75$) were found between the parameter ALA and the parameters ALL, ALW and ALP (Table 5). These correlations are also high in the analysis of EW only or LW only (Table 6 and Table 7). In EW, there is an almost perfect correlation between eALL and eACL. This correlation in LW is quite high but not as good as in EW. In LW, the highest correlation was found between lACL and lAWT. This correlation is characteristic of LW; in EW, the correlation between eACL and eAWT is indeed very low.

Even comparing other chronologies of anatomical parameters gives very different results between EW and LW. The correlations between AFC and ALA, ALL and ALW show clearly different results in EW and LW. In EW, the correlations between these factors are almost non-existent, while in LW, they are moderately positive. The same is also true for the correlations between AWT, ALL and ALLW.

Table 5: Correlation coefficients (Pearson's r) of the detrended wood anatomical parameters for the entire ring (1731–2013). Significant correlations are indicated by asterisks (p-value < 0.05).

	RW1	RW2	%LA	ALA	ALL	ALW	ALP	AFC	ALLW
RW1									
RW2	0.772*								

%LA	0.291*	0.222*							
ALA	0.299*	0.140*	0.582*						
ALL	0.315*	0.173*	0.390*	0.891*					
ALW	0.235*	0.175*	0.428*	0.809*	0.538*				
ALP	0.299*	0.150*	0.479*	0.789*	0.745*	0.587*			
AFC	0.078	0.197*	0.050	0.222	0.197*	0.399*	-0.291*		
ALLW	0.123*	0.002	0.063	0.325*	0.642*	-0.245*	0.338*	-0.167*	

Table 6: Correlation coefficients (Pearson's r) of the detrended wood anatomical parameters for EW. Significant correlations are indicated by asterisks (p-value < 0.05).

	RW1	**RW2**	**eALA**	**eALL**	**eALW**	**eACL**	**eALP**	**eAFC**	**eALLW**	**eAWT**
RW1										
RW2	0.772*									
eALA	0.225*	0.538*								
eALL	0.199*	0.023	0.850*							
eALW	0.223*	0.117*	0.7743	0.347*						
eACL	0.178*	0.010	0.782*	0.969*	0.275*					
eALP	0.173*	0.016	0.730*	0.677*	0.514*	0.623*				
eAFC	0.042	0.113	-0.046	-0.172*	0.137*	-0.167*	-0.658*			
eALLW	-0.069	-0.144*	0.135*	0.600*	-0.508*	0.621*	0.207*	-0.317*		
eAWT	-0.053	-0.021	-0.212*	-0.079	-0.227*	0.165*	-0.168*	0.023	0.064	

Table 7: Correlation coefficients (Pearson's r) of the detrended wood anatomical parameters for LW. Significant correlations are indicated by asterisks (p-value < 0.05).

	RW1	**RW2**	**lALA**	**lALL**	**lALW**	**lACL**	**lALP**	**lAFC**	**lALLW**	**lAWT**
RW1										
RW2	0.772*									
lALA	0.125*	0.226*								
lALL	0.182*	0.275*	0.888*							
lALW	-0.095	0.021	0.718*	0.464*						
lACL	0.235*	0.233*	0.579*	0.734*	0.085					
lALP	0.202*	0.238*	0.724*	0.667*	0.473*	0.443*				
lAFC	-0.086	0.067	0.530*	0.474*	0.626*	0.197*	-0.089			
lALLW	0.261*	0.205*	0.079	0.413*	-0.508*	0.611*	0.168*	-0.245*		
lAWT	0.220*	0.172*	0.302*	0.452*	-0.123*	0.936*	0.237*	0.022	0.589*	

Blue intensity

Earlywood blue intensity (EWBI), latewood blue intensity (LWBI) and ΔBI (difference between EWBI and LWBI) correlate better with RW1 than with anatomical parameters (the correlation coefficients are -0.564, 0.221 and 0.702, respectively). However, EWBI has very similar correlations to RW1 and anatomical parameters when calculated only for EW or for the whole ring. Only the anatomical parameters eAFC, AFC and eAWT do not correlate significantly with EWBI (Figure 23).

The correlations for ΔBI are slightly lower with anatomical parameters (calculated for only EW and for the whole ring) than with RW1. However, they are all significant except for the correlations between ΔBI and eALW, eAFC, AFC and eAWT. Of all the parameters, the one showing the best correlations with EWBI and ΔBI are ALL and eALL (Figure 23).

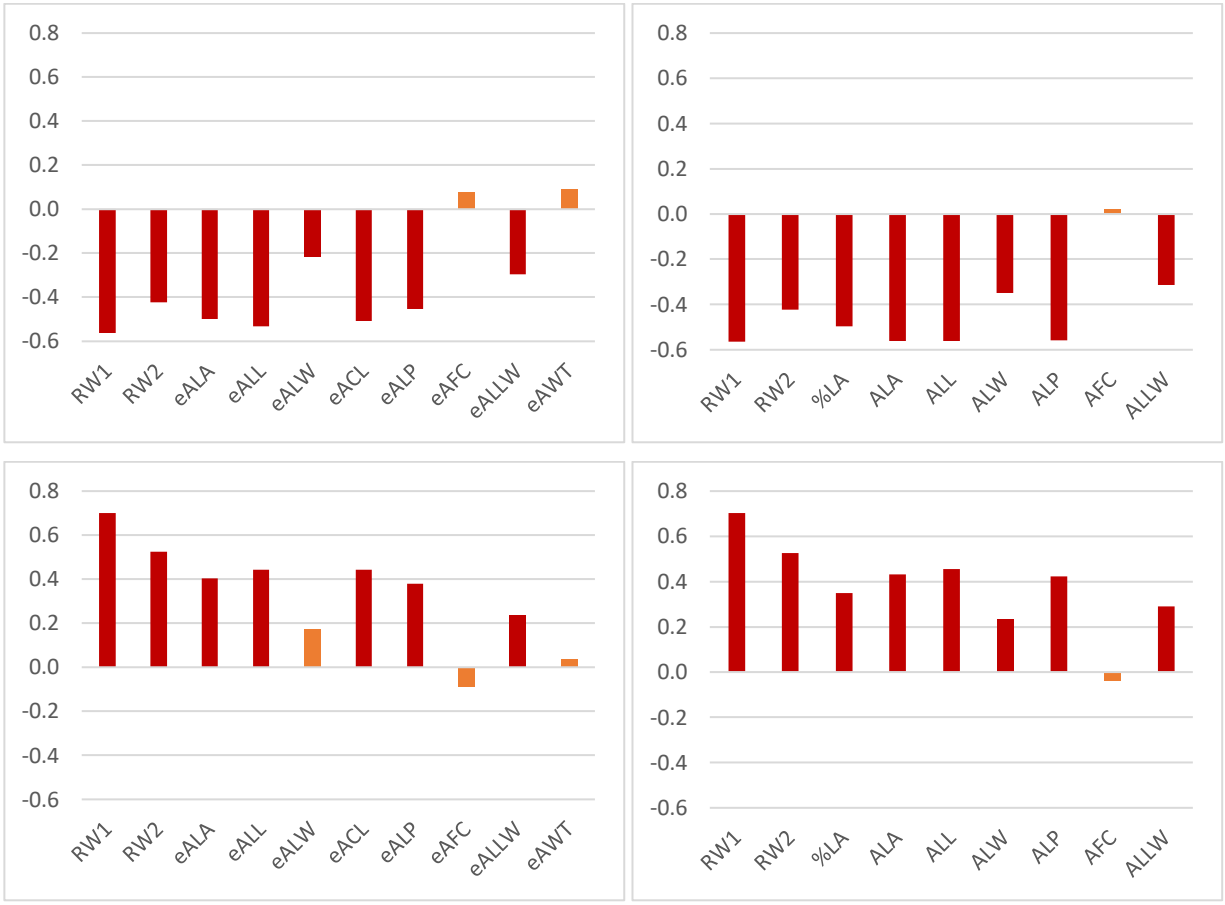

Figure 23: Coefficients of correlations between earlywood blue intensity (EWBI; top) or ΔBI (bottom) and the wood anatomical parameters (only for EW on the left; for the entire ring on the right) for the years 1900–2012. Correlations in red are significant (p-value < 0.05).

Among the three blue intensity parameters, LWBI is the one that has the worst correlations (correlation coefficient < |0.220|) with the anatomical parameters. No correlation between LWBI and anatomical parameters (whether calculated for EW only, LW only or the whole ring) is significant. However, the LW anatomical parameters show significant correlations with both EWBI and ΔBI. In the case of LW, lALL shows

no better correlations than the other anatomical parameters. The LW anatomical parameter that correlates better with the BI parameters is lAWT, a parameter that in the case of EW and the whole ring had low (and sometimes even non-significant) correlations.

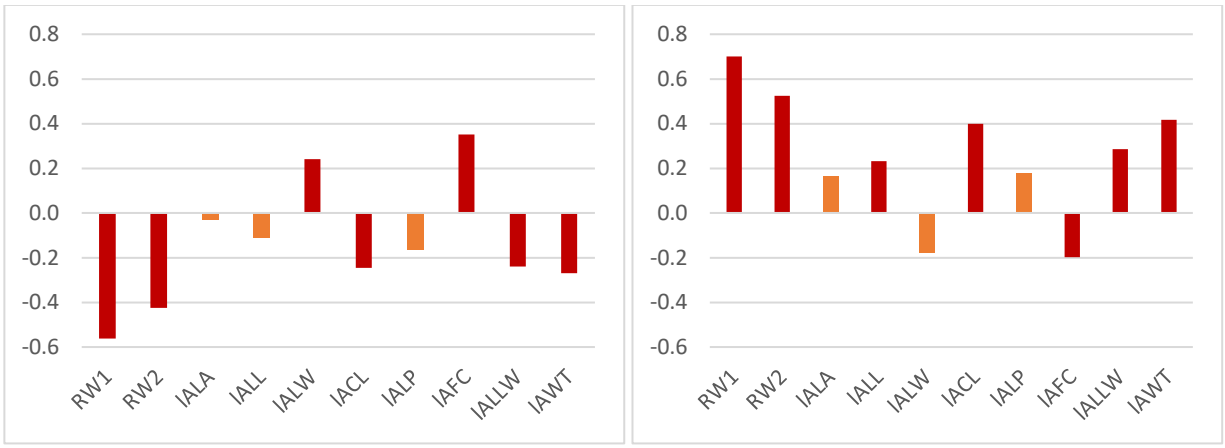

Figure 24: Coefficients of correlations between EWBI (left) or ΔBI (right) and the LW wood anatomical parameters for the years 1900–2012. Correlations in red are significant (p-value < 0.05).

Wood anatomical data and climate

Correlations with precipitation

The analysis of the Pearson's r of the correlations between three-monthly precipitation, ring width and the wood anatomical parameters (Table 11, Table 12 and Table 13) shows that the wood anatomical parameters have higher correlations with precipitation than ring width does. The best correlation between ring width and rainfall is with the sum of the rain that fell in previous NDJ months (r = 0.4076).

The wood anatomical chronologies calculated for the entire ring show coefficients of correlation of up to 0.4975 (ALA and OND precipitation). ALA shows significant and high correlation only in the two periods SON and OND; in the following three-monthly periods, the correlation coefficient tends to be lower and lower (Figure 25).

In the period OND of the year prior to the year in which the ring was dated, when ALA shows the highest correlation, four out of seven wood anatomical parameters have significant correlations with precipitation (Figure 26).

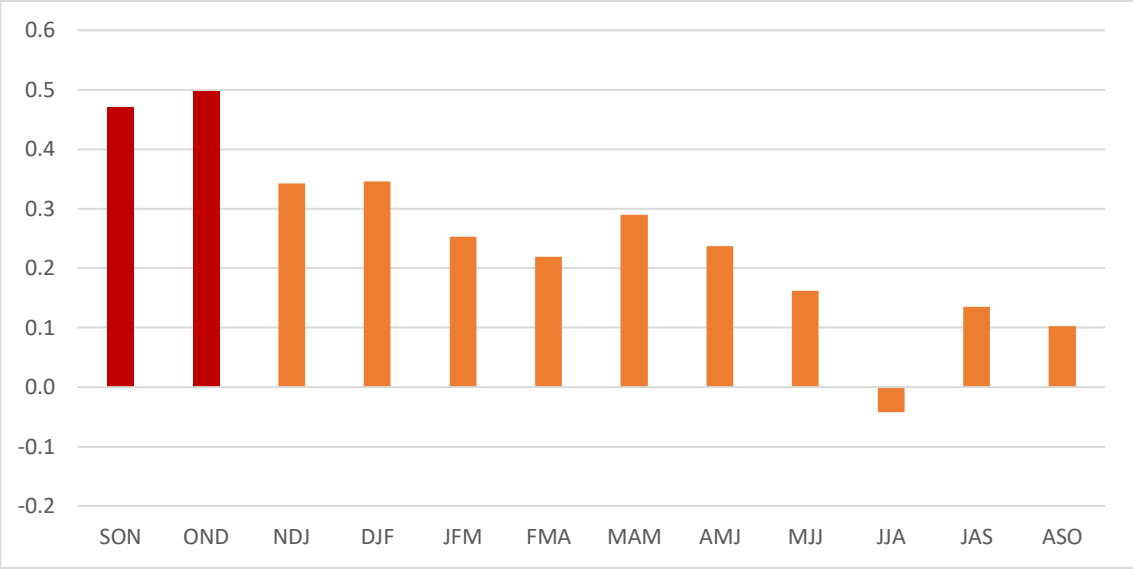

Figure 25: Coefficients of correlation between ALA and precipitation during three-monthly periods (1980–2006). Significant correlations (p-value < 0.05) are in red.

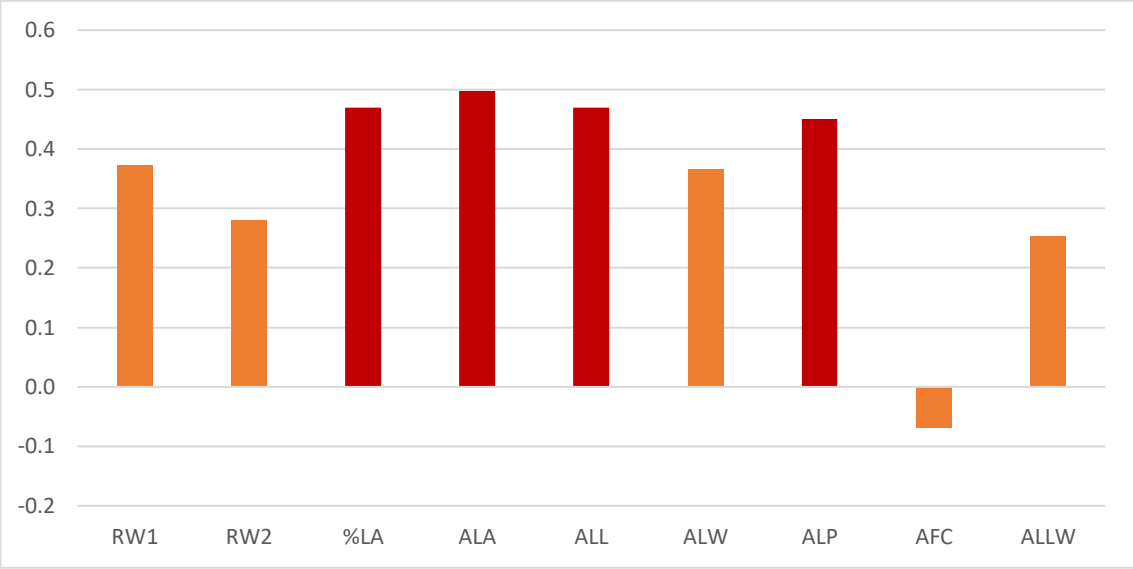

Figure 26: Coefficients of correlation between OND precipitation and anatomical parameters (entire ring, 1980–2006). Significant correlations (p-value < 0.05) are in red.

EW anatomical parameters show higher correlations with precipitation than the parameters calculated for the entire ring does (Table 11 and Table 12). The highest correlation that has been found is between eALA and rainfall over the months of SON of the year prior to the year in which the ring was dated (0.5393). Similar to what is observed for ALA, the values of the correlation coefficients between eALA and precipitation also tend to decrease during the year (Figure 27). The four parameters eALA, eALL, eACL and eALP show correlations above 0.4400 only for the months of the previous autumn (SON or OND), and the parameters ALW, AFC, ALLW and AWT show generally lower correlations than the other parameters (Figure 28).

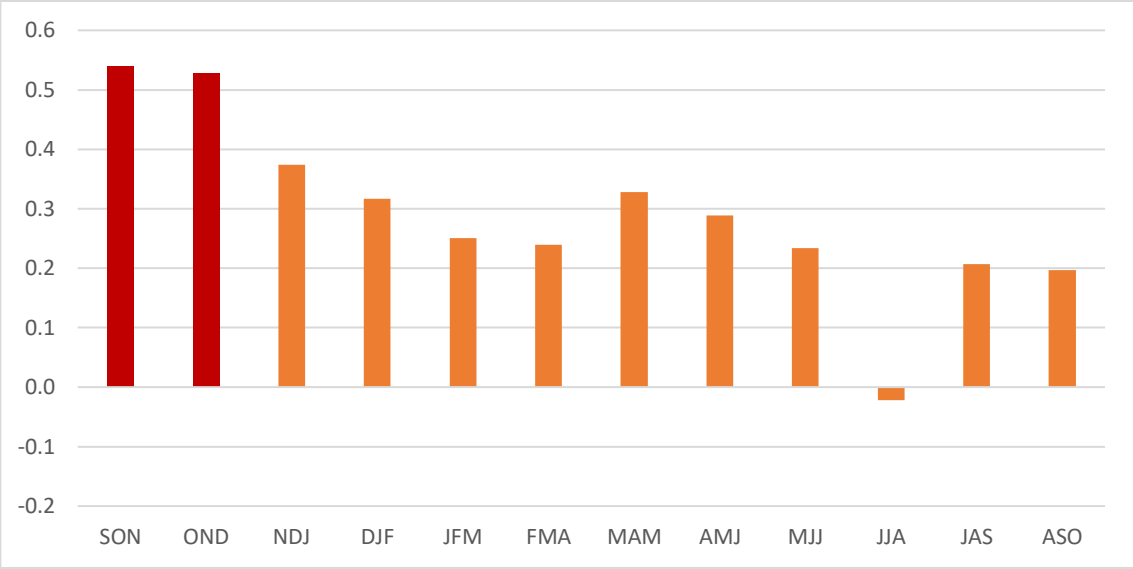

Figure 27: Coefficients of correlation between eALA and precipitation during three-monthly periods (1980–2006). Significant correlations (p-value < 0.05) are in red.

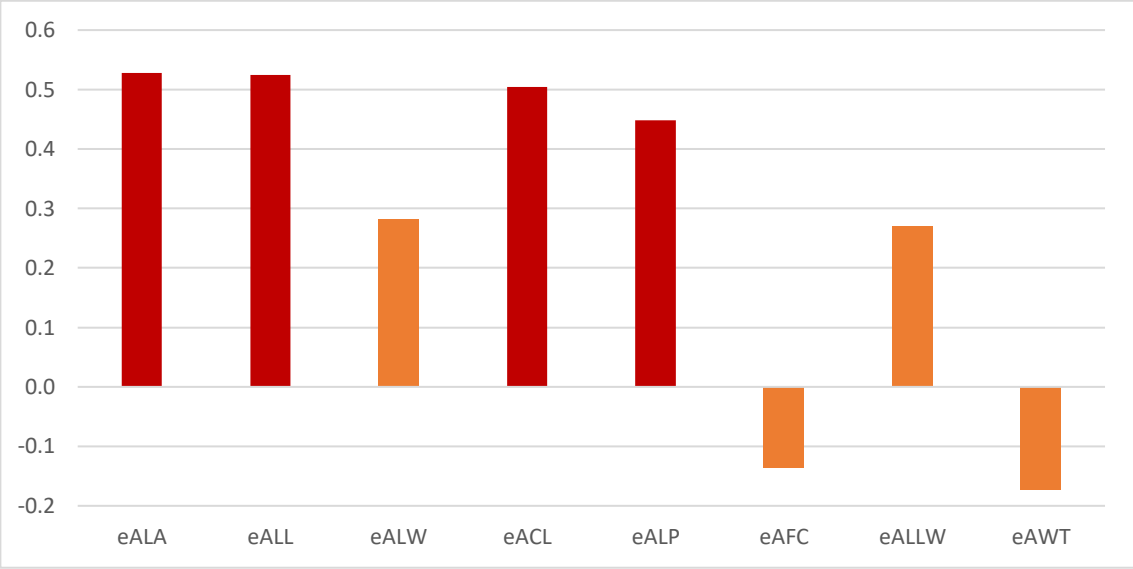

Figure 28: Coefficients of correlation between OND precipitation and EW anatomical parameters (1980–2006). Significant correlations (p-value < 0.05) are in red.

The coefficients of correlation between precipitation and the LW anatomical chronologies are lower than those presented previously. Only one correlation is higher than 0.4400 (lALA and AMJ precipitation). In the case of LW, the correlation coefficient of lALA changes during the year in a different way than do those of the parameters ALA and eALA, which had the highest values in the previous autumn and then tended to decrease over the course of the year. In the case of lALA, the highest peak occurs in the spring period (especially in the months of AMJ), while the trend over the rest of the year is not clear (Figure 29).

It can be observed that lALA, lALL, lACL and lALP, which are the parameters that have the highest correlations whether those correlations are calculated for the entire ring or only for EW cells, are the parameters that

also, in this case, show the highest correlations. All four parameters have correlations with coefficients higher than 0.3000 almost exclusively with the sum of rainfall in the period AMJ (Figure 30). The only two significant correlations between precipitation and LW anatomical parameters are those between lALA and AMJ precipitation and lALL and AMJ precipitation. Even in this case, the parameters ALW, AFC, ALLW and AWT show low correlation with precipitation.

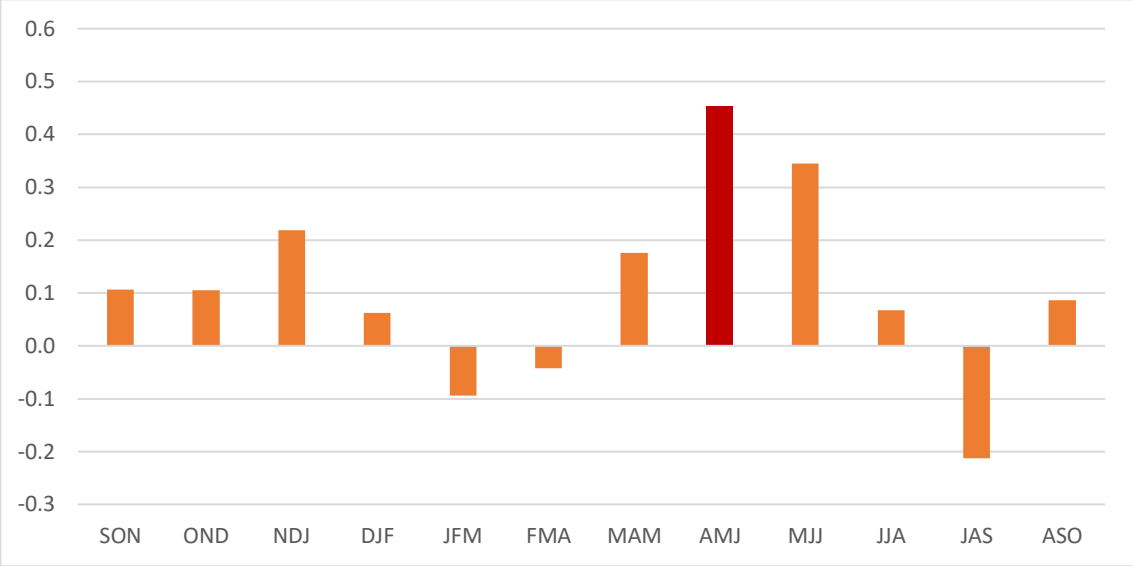

Figure 29: Coefficients of correlation between lALA and precipitation during three-monthly periods (1980–2006). Significant correlations (p-value < 0.05) are in red.

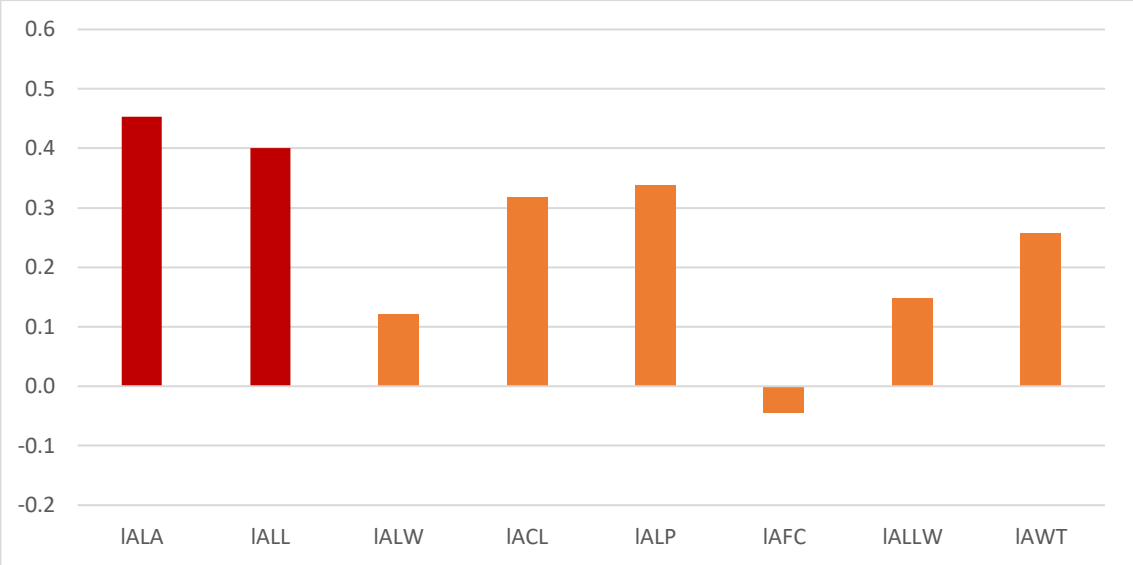

Figure 30: Coefficients of correlation between AMJ precipitation and EW anatomical parameters (1980–2006). Significant correlations (p-value < 0.05) are in red.

With a linear model based on the correlation between eALA and SON precipitation, the SON precipitation values have been reconstructed. The median residual of this linear model is -128.4 and the R^2 is 0.29. In Figure 31, the comparison between measured and reconstructed precipitation can be observed.

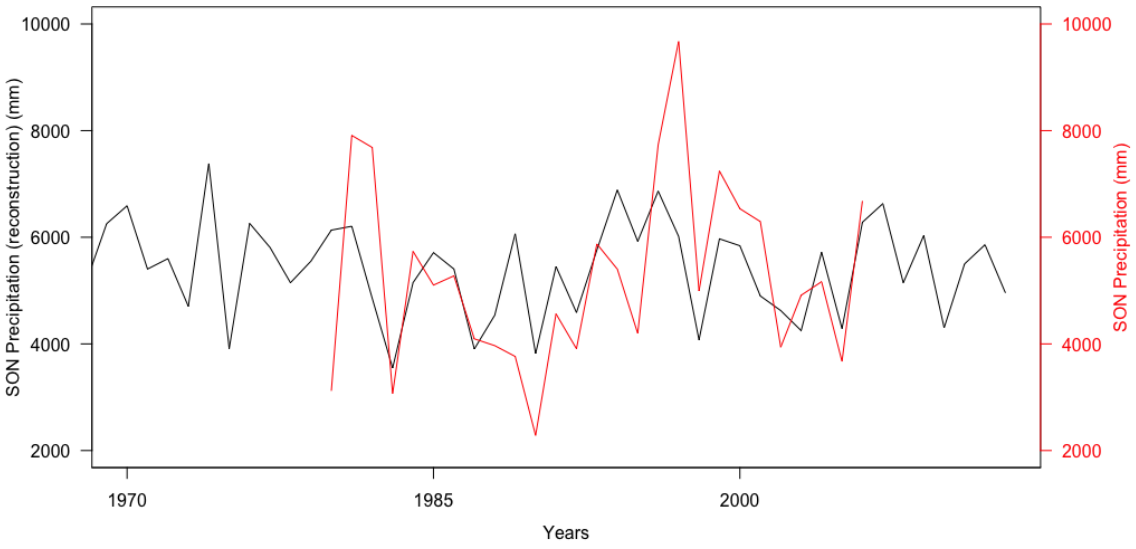

Figure 31: Comparison between the measured and reconstructed SON precipitation values.

The trend of temperatures over the last three centuries (Figure 32) shows great variation from year to year. Years with particularly high or low rainfall are present at regular intervals. The extreme events in the first years of reconstruction (until 1733) may be amplified since they are based on only one core. In the medium-long term, no trend can be observed due to the type of detrending that was applied to the anatomical data.

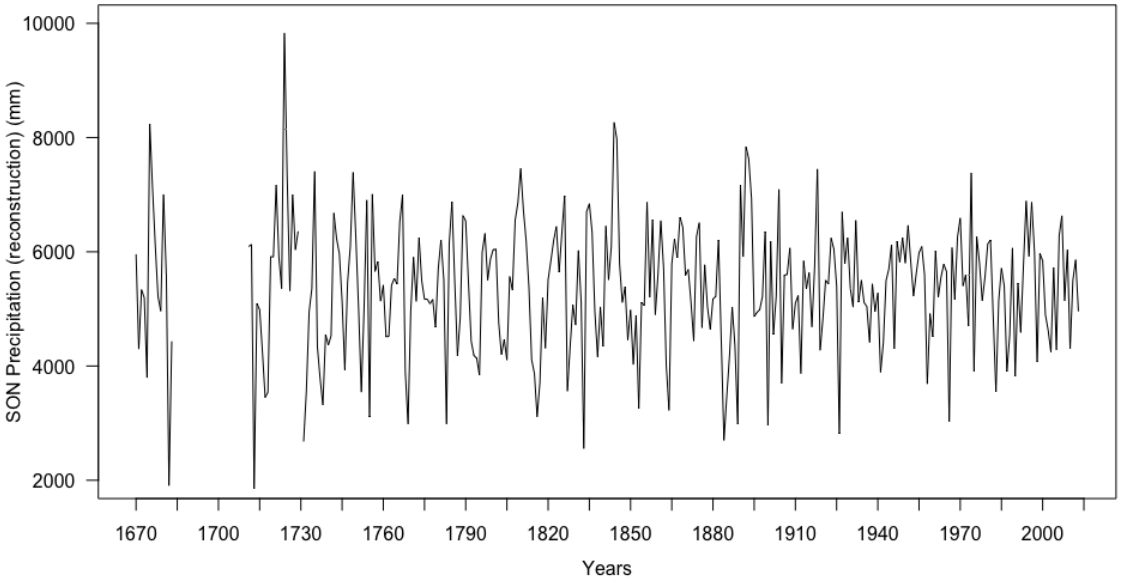

Figure 32: Reconstruction of SON precipitation.

The years with less SON rainfall, according to this reconstruction, are 1682, 1713, 1731, 1833, 1844 and 1926 (SON rainfall ≦ 2,800 mm); those in which it rained the most in SON are 1675, 1724, 1844, 1845, 1892 and 1893 (SON rainfall > 7,500 mm). Among the six years with more rainfall in SON, they occur consecutively at two points (1844–1845 and 1892–1893).

Correlations with Standardized Precipitation Evapotranspiration Index

The anatomical parameters have low correlations (< |0.25|) with the monthly Standardized Precipitation Evapotranspiration Index (SPEI) data for the period 1911–2012. Only the SPEI data for April are an exception and show higher correlations (Table 8). The parameter ALP best correlates with the April SPEI data (r = 0.4704). This correlation is considerably higher than that between the April SPEI data and RW1 (r = 0.3137). Almost all the correlations between the April SPEI data and the parameters of the entire ring or EW are significant; those with the LW parameters are significant for only three anatomical parameters.

Table 8: Coefficients of correlation between the April Standardized Precipitation Evapotranspiration Index (SPEI) data of the sampling site (1911–2012) and the anatomical parameters. Significant correlations (p-value < 0.05) are marked by asterisks.

	Entire ring	Earlywood	Latewood
RW1	0.3137 *		
RW2	0.2981 *		
%LA	0.4241 *		
ALA	0.4450 *	0.4050 *	0.0476
ALL	0.4313 *	0.4107 *	0.0963
ALW	0.2868 *	0.2348 *	-0.1791
ACL		0.3601 *	0.1637
ALP	0.4704 *	0.4124 *	0.2016 *
AFC	-0.1658	-0.2684 *	-0.4029 *
ALLW	0.2884 *	0.2541 *	0.2362 *
AWT		-0.2358 *	0.1699

The April SPEI data were reconstructed using a linear model based on the correlation with ALP. The linear model is characterized by a median residual equal to -0.03748 and an R^2 of 0.221.

Figure 33 shows a comparison of measured and reconstructed values over a period of about 45 years. For some years, the model approximates badly the values (e.g., 1945 and 1955), but in general, the variations between the years are well represented.

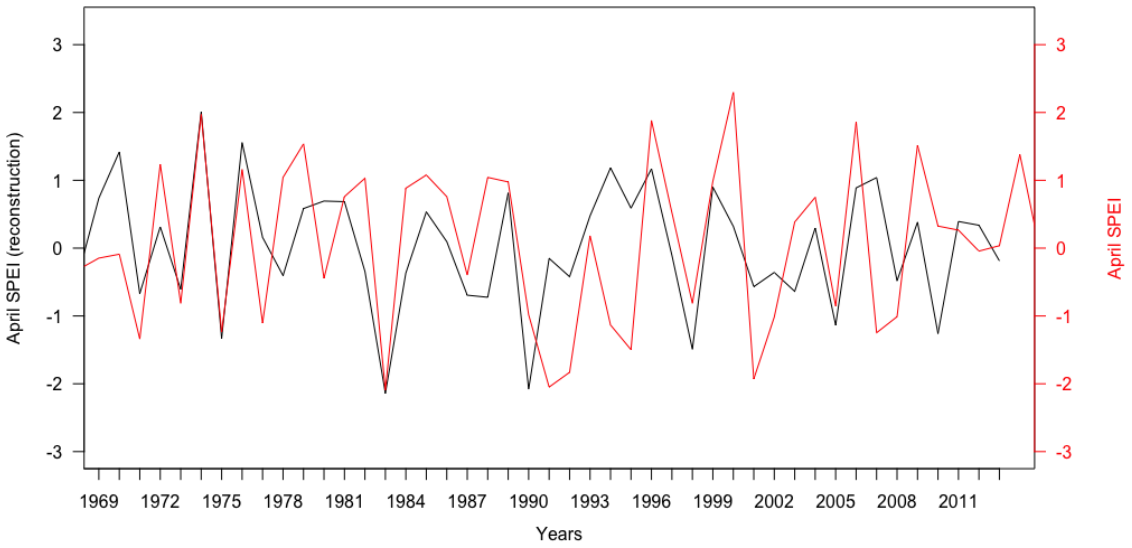

Figure 33: Comparison between the measured and reconstructed April SPEI data.

Looking at the reconstruction made for the period 1670–2013 (Figure 34), observations can be made that are similar to those made for the reconstruction of SON precipitation. Due to the type of detrending carried out on the eALP data, it is not possible to observe medium- or long–term trends, but it is possible to observe frequent variations from year to year.

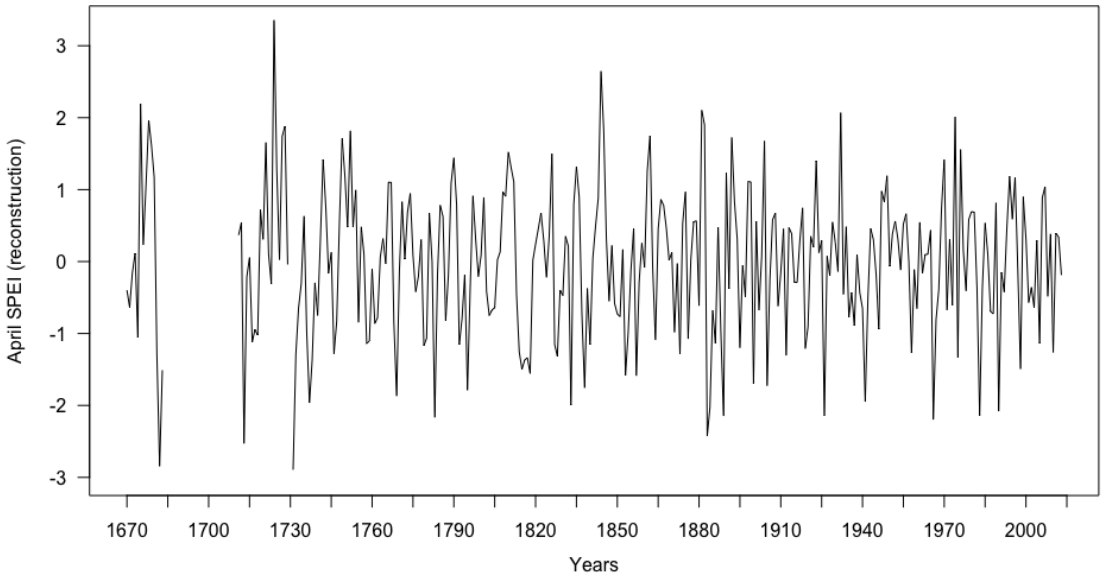

Figure 34: Reconstruction of the April SPEI data.

The years in which the April SPEI data were lower, according to the reconstruction, are 1682, 1713, 1731, 1783, 1883 and 1966 (< -2.15). The years in which the April SPEI data were higher were 1675, 1724, 1844, 1881, 1932 and 1974 (> 2.00).

Correlation with maximum temperature

By analysing the maximum monthly temperature with the anatomical parameters, high correlations were found almost solely in April, similarly to the results found between the April SPEI data and the anatomical parameters. Only by comparing the anatomical data with the maximum temperatures in April could correlation coefficients of more than 0.30 be found. Most of these correlations are highly significant. The maximum correlation coefficient (r = -0.4343) is between the maximum temperature in April and the eALP and is higher than the correlation between maximum temperature in April and RW1 (-0.2897).

Table 9: Coefficients of correlation between the April maximum temperature of the sampling site (1902–2013) and the anatomical parameters. Significant correlations (p-value < 0.05) are marked by asterisks.

	Entire ring	Earlywood	Latewood
RW1	-0.2897 *		
RW2	-0.2960 *		
%LA	-0.3719 *		
ALA	-0.3925 *	-0.4145 *	-0.0229
ALL	-0.3677 *	-0.3960 *	-0.0982
ALW	-0.2445 *	-0.2748 *	0.2666 *
ACL		-0.3600 *	-0.1915 *
ALP	-0.4218 *	-0.4342 *	-0.1879 *
AFC	0.1775	0.2694 *	0.4238 *
ALLW	-0.2555 *	-0.1961 *	-0.2769 *
AWT		0.1762	-0.2093 *

By correlating the maximum temperature data averaged over three months, correlations were obtained that slightly exceed 0.30 even in other times of the year. However, the highest correlations even when analysing the averaged climate data are those for the spring period (months MAM). The climate parameter that correlates best with the maximum temperature is confirmed to be the eALP.

Also, the maximum temperatures of April were reconstructed with a linear model based on the best correlation with an anatomical parameter – in this case, the eALP. Although the model may not seem to approximate the observations well (Figure 35), the median residual is 0.00778. The R^2 is 0.1858.

The entire reconstruction of the maximum temperatures in April is shown in Figure 36. Also, for this reconstruction, similar observations to those made of the other two are valid. Because of the detrending

done on the eALP parameter, no medium- or long–term trends are recognizable, but frequent and important variations from year to year are observed.

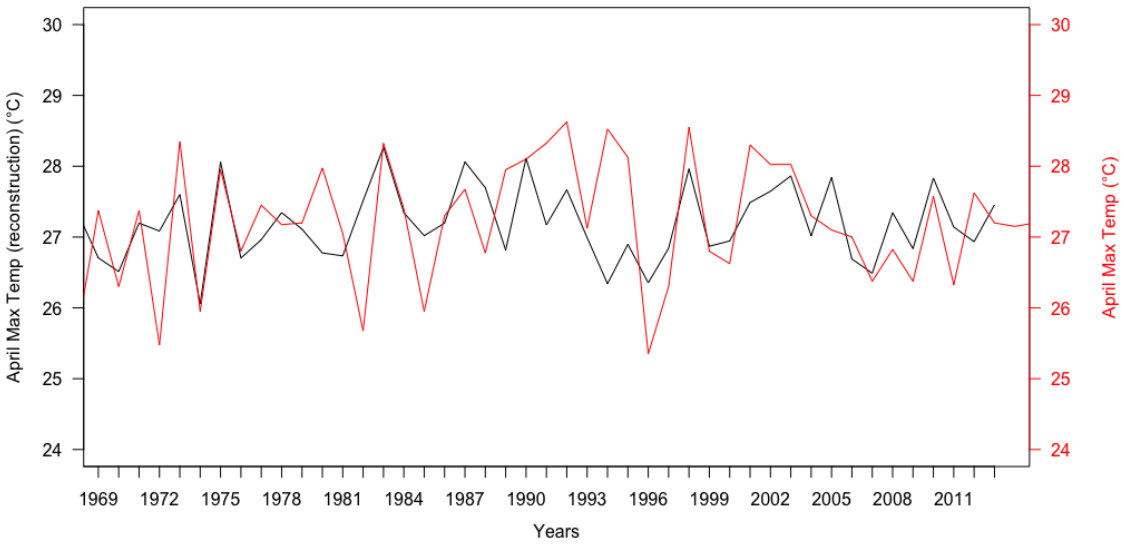

Figure 35: Comparison between the measured and reconstructed April maximum temperatures.

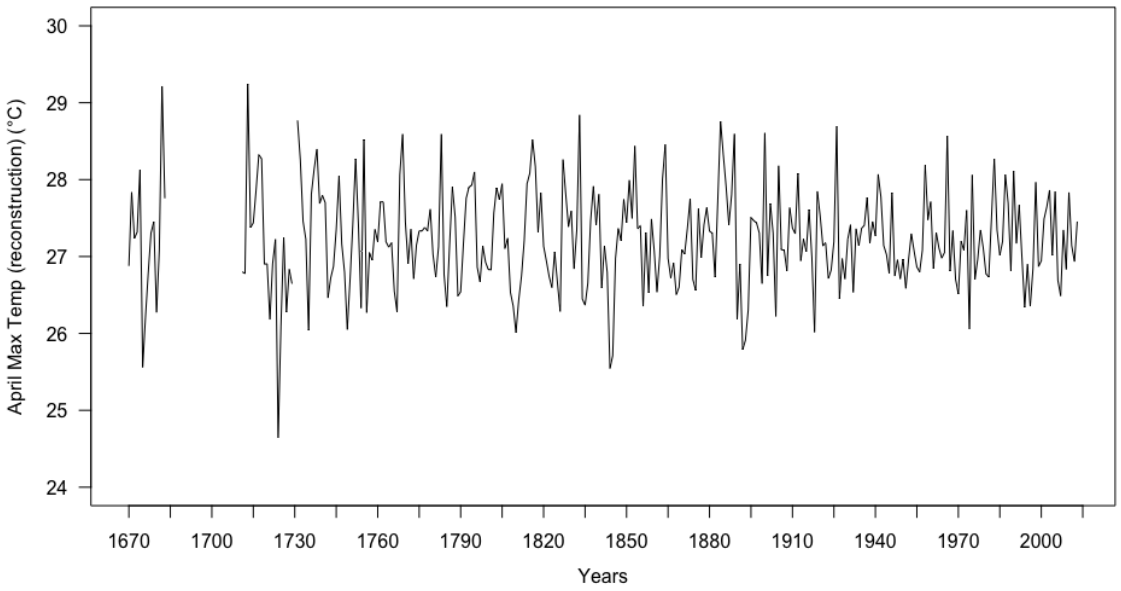

Figure 36: Reconstruction of the April maximum temperatures.

The years in which the maximum temperatures in April were lower (< 26.00°C) were 1675, 1734, 1844, 1845, 1892 and 1893. Among the six years with lower April maximum temperatures, they occur consecutively at two points (1844–1845, 1892–1893). These two pairs of years are the same pairs of years in which, according to the reconstruction made of SON precipitation, rainfall was very high in the SON months.

The years with the highest maximum temperatures in April were 1682, 1713, 1731, 1833, 1884 and 1926 (> 28.65°C).

Discussion

Methods

Two different instruments and two different methods to avoid cell walls breaking were used to prepare the microsections. The first method tested was embedding the samples into the paraffin and cutting the microsections with the rotatory microtome. Embedding the samples in paraffin should have prevented damage to the cell structure (Von Arx et al., 2016). However, this method did not produce the expected results. In fact, paraffin did not penetrate all the cells, and some were reinforced by the presence of paraffin, while others were not (Figure 37). During cutting with the rotatory microtome, most of the cell walls, presumably especially those of the cells that were not filled with paraffin, were broken or damaged. As a result, the image quality that could have been obtained from these microsections would not have been sufficient to perform the analysis. Moreover, the fact that it was not possible to choose the cutting direction probably influenced the quality of the microsections obtained.

Breakage or separation of the secondary cell wall during microsection cutting is a known problem that mainly concerns the earlywood (EW) of conifers (Schneider & Gärtner, 2013). The broken cell walls bend in the cell lumens and usually compromise the image analysis of several wood anatomical parameters (Schneider & Gärtner, 2013). The breakage of cell walls can be due to several factors: low cell wall densities, sample sizes, microtome blade orientation, human experience and dexterity and unsuitable blades (Schneider & Gärtner, 2013). However, paraffin embedding should prevent the described problems. In the analysed samples, contrary to what Schneider and Gärtner (2013) report, paraffin did not fill all the cells on the surface of the wood sample (Figure 37).

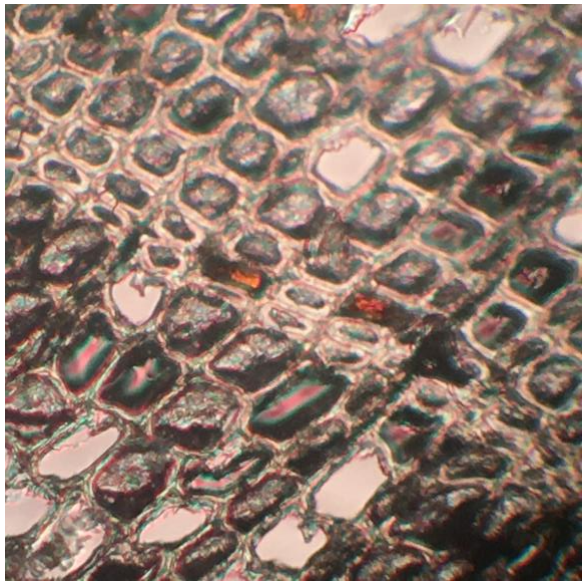

Figure 37: Paraffin did not fill all the cells.

There are alternative methods to the use of paraffin to prevent cell walls from breaking, such as using a solution of starch and water or soaking (or boiling) the samples in water (Von Arx et al., 2016). The solution of corn starch and water forms a shear-thickening non-Newtonian fluid. This means that when the solution is exposed to pressure, it becomes solid and stabilized. When distributed on the surface to be cut, the starch solution fills the exposed tracheids, and when cutting, the blade exerts pressure on the solution. Consequently, the sample reacts to the cut as a homogeneously full wooden material and not as a piece of wood with pores filled with air or a liquid solution (Schneider & Gärtner, 2013). In addition to the technical aspects, the other advantages of using a starch-based solution are that the solution is non-toxic, inexpensive

and easy to obtain and that it does not damage the blade or the wood sample (Schneider & Gärtner, 2013). In comparison with corn starch, rice starch has a smaller grain size and therefore is also suitable for small cells (Von Arx et al., 2016). However, using rice starch with the *Fokienia hodginsii* samples did not give results that were as good as the results given when corn starch was used.

Better microsections were likely obtained not only by the change of method to avoid cell wall breakage but also by the change of microtome type. For most of the samples embedded in paraffin, a rotary microtome was used, and for the rest, a sledge microtome was used. Gärtner et al. (2014) underline the importance of the quality of the microtome for plant anatomical research and the fact that this topic has not been at the centre of research on new analytical techniques, which mostly focus on microscopy or image analysis.
Currently, rotary microtomes are very common but are designed primarily for human tissues. The samples must be embedded in the paraffin to get a good-quality microsection because the blade puts pressure on the sample without truly cutting it (Gärtner et al., 2014). Preparing samples with paraffine takes a long time compared to preparing them with starch. To remove paraffin, it is necessary to use xylol, a flammable and toxic solvent.
During the laboratory work carried out for this thesis, another disadvantage of this instrument emerged: the positions of the blade and the sample can be changed very little. The other side of the coin is that is possible to obtain microslides with a very standardized process; it is easy to keep the same settings for all the samples and to set with great precision the thickness of the sample to be cut. If the type of wood is suitable for this type of microtome (not dense wood), it is feasible that one can quickly cut many microsections.
The sledge microtome that was used after the rotary microtome failed is designed to cut a variety of types of wood. It allows one to set their desired angle of the blade to the sample.

Wood anatomical characterization of *Fokienia hodginsii*

The Vietnamese conifer *Fokienia hodginsii* differs from most other conifers growing in the tropics because of its distinct ring boundaries. According to Baas, Pieter et al. (2004), in fact, conifers growing in tropical regions often do not show distinct growth ring boundaries, while those growing in temperate zones do. This anatomical (and physiological) characteristic allows for successful dendroclimatic studies.

The differentiation between EW and LW in each ring makes it possible to isolate the climatic signal on an intra-annual level. In addition, the differentiation between EW and LW is necessary to avoid a loss of information. For example, analysing the ALA of an entire ring makes little sense, since the ALA is an average among many cells belonging to two categories of cells with different forms and functions and growing at different times of the year. Figure 38 shows the differentiation between EW and LW in a sample. Each cell is represented by a blue or red dot; because of this differentiation, is possible to recognize the tree rings.

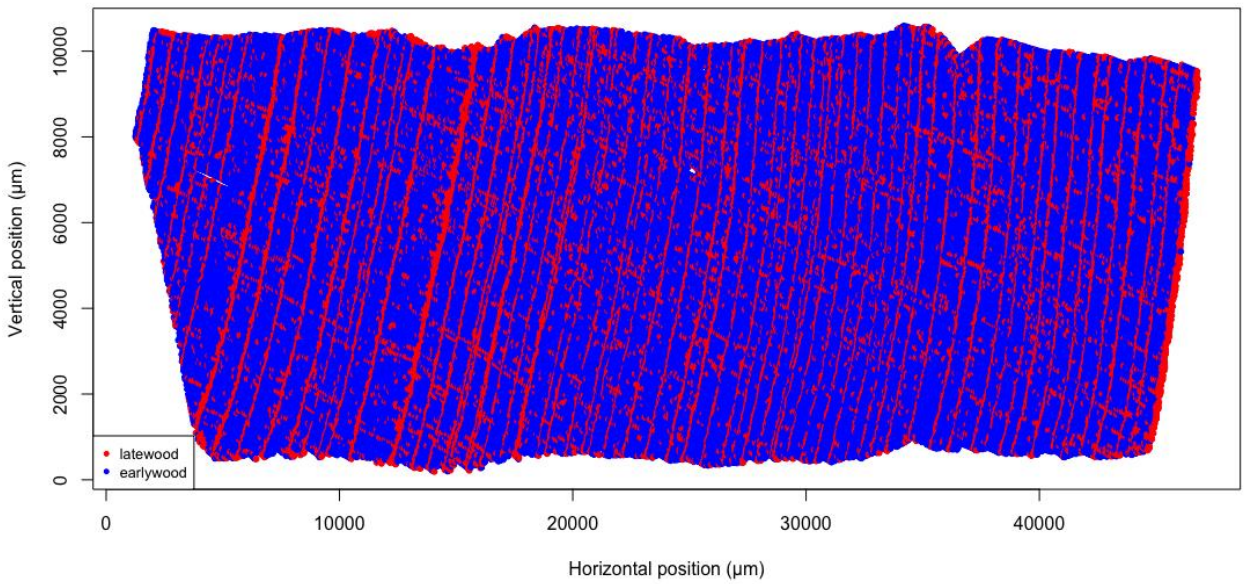

Figure 38: Early- and latewood differentiation in sample TGFH10B1. Every cell is represented by a dot.

The mathematical formula that takes into account cell wall thickness and lumen length approximates well the differentiation between EW and LW; however, there are errors due to the presence of small cells inside the EW (and vice versa, although to a lesser extent). Another source of error in this approximation is due to WinCELL's difficulty in recognizing very small cells: the LW data consequently have a higher inaccuracy than the EW data do.

High correlations between wood anatomical parameters were expected. ALW and ALL are the two parameters that most define the shape and size of the lumen and on which other parameters (in particular, ALP and ALA) depend. Between ALA and ALW or ALL (even only for EW or LW), very high correlation coefficients have been calculated (between 0.7 and 0.9). The correlations are slightly higher between ALA and ALL than between ALA and ALW; as also observed qualitatively, the cell width varies less than the length. ALP also correlates well primarily with ALA and secondly with the ALA components ALL and ALW.

Another correlation that was expected to be very high is the one between ACL and ALL. These two parameters differ for cell walls, which are included in ACL but not in ALL. The correlation is higher in EW than in LW, where the ratio between cell walls thickness and lumen length is much larger. This feature of LW cells also explains the very high correlation between lACL and lAWT (r = 0.936). Except for this correlation and that between lAWT and lALLW (also caused by the fact that the length of an LW cell is determined mainly by the thickness of cell walls), AWT does not correlate well with any parameter.

The %LA has a good correlation with ALA (0.582) and, consequently, also with the parameters that define ALA (ALL, ALW and ALP). This correlation was expected, as the percentage of area occupied by the lumens in a ring is higher if there are few cells rather than many (assuming that the cell wall thickness remains the same).

On a quantitative level, there are clear differences between EW and LW cells (Figure 15). These differences are driven by the need for tracheids that perform two different main functions: delivering water to the tree canopy and providing mechanical support. This dual role is an ancestral characteristic of tracheids, compared to angiosperm xylem cells, which specialize in one of two functions. However, this characteristic does not represent a clear evolutionary disadvantage; on the contrary, some conifers are among the oldest eukaryotes in the world (Hacke et al., 2015).

Axial parenchyma

Parenchyma cells form one of the main tissues of which plants are composed. This type of cell can be found in every organ of plants and can perform different types of functions (Morris, 2016). In xylem, parenchyma cells in the secondary cell wall can be lignified and oriented as the tracheids (axial parenchyma) or radially (ray parenchyma). This characteristic makes it very difficult to distinguish axial parenchyma from tracheids (Morris, 2016). For this thesis, axial parenchyma cells were only recognized when they had content within them.

The visual analysis carried out (Figure 19) does not show that axial parenchyma bands are formed in the same years in the various samples. However, the analysis has many limitations. The first main limitation is that the analysis was carried out on only five cores over a period of 68 years, and for each year, there were only two or three tree rings from the five cores; the sample size is therefore very small.

The second main limitation is that the substance that fills the axial parenchyma cells does not fill all the cells and does not fill the cells completely (Figure 18). This means that not all axial parenchyma cells are distinguishable from tracheids. Consequently, it cannot be concluded with certainty that axial parenchyma cells bands do not occur in correspondence with certain climatic or environmental conditions.

Plavcová and Jansen (2015) show that tropical trees grown under the same conditions accumulate starch in parenchyma cells in different amounts; differences were also observed between tree parts. In addition, it is possible that these substances have been mobilized or consumed between the time of their formation and the time of sample extraction and that those found do not coincide with those produced in the year of cell formation. This possibility, therefore, may disprove the fact that the content of axial parenchyma cells is not formed with specific environmental conditions in the year of cell formation and that only part of it is currently still in the cells.

Plavcová and Jansen (2015, p. 212) state that 'in gymnosperms, the total parenchyma proportions are commonly between 5 and 10% and compose mainly of radial parenchyma". In this study, it was not possible to quantify parenchyma cells, which could exceed the estimate made by Plavcová and Jansen (2015). O'Brien et al. (2014) reported a higher percentage of axial parenchyma cells in the total number of parenchyma cells in tropical trees and higher total parenchyma proportions in plants growing in tropical (rather than in temperate) zones. It is also known that in the Cupressaceae family, to which *Fokienia hodginsii* belongs, axial parenchyma is a common feature (Baas, Pieter, et al., 2004).

Although the qualitative analysis did not give any indication of storage of substances in the same years in different trees, the feature of having these tangentially zonate parenchyma bands should be further analysed from a chemical and functional point of view. Until now, features related to the support and storage functions as parenchyma cells have not been studied in depth, not only for *Fokienia hodginsii* but also for other species, although these features may reveal information about environmental conditions (Eckstein, 2013). In the case of *Fokienia hodginsii*, it remains unclear, for instance, which substance fills the axial parenchyma cells, what its role is and whether parenchyma cells are formed regularly or as a result of certain conditions.
A further open question concerns the position of axial parenchyma bands (at the beginning of the ring, in the middle of the EW, between the EW and the LW and in the LW). The visual analysis carried out shows that in the period 1946–1980, the bands are mainly found in LW, while in the period 1981–2013 they are located mainly in EW. The cause of this distribution is not clear.

O'Brien et al. (2014) demonstrated that the storage of non-structural carbohydrates (NCSs) is a feature that positively impacts tropical trees' resistance to and resilience during climate change–induced drought. This category of substances, which includes, for example, sugars and starches, is the most stored in parenchyma (Plavcová & Jansen, 2015). If also in the case of *Fokienia hodginsii* the substances contained in the cells are NCSs, it might be interesting, for example, to verify on a very long-term scale how the distribution of full axial parenchyma cells varies or to verify the distribution in relation to particularly dry years.

Blue intensity

Buckley et al. (2018) interpreted the blue intensity (BI) as a proxy of tree ring density. The anatomical parameter analysed in this thesis that theoretically could better reflect tree ring density is %LA. This parameter expresses the percentage of the area occupied by lumens in a ring. Therefore, 1-%LA corresponds to the percentage of area occupied by cell walls. To obtain the density of the tree ring, however, the specific weight of the cell wall must still be considered. The latter depends on the content of the relative abundance of the three macromolecular classes (celluloses, hemicellulose and lignin) but should be more or less constant

among tree species (~1.5 g/cm^3, Björklund et al., 2019). However, the correlation between the three BI parameters measured by Buckley et al. (2018) and %LA is lower than expected. It must be considered that the %LA parameter has been measured only for the whole ring and not separately for EW and LW and that BI data was not measured for the whole ring but for EW and LW separately (plus the difference between these two data). This certainly influences the correlations.

Buckley et al. (2018) consider the possibility that 'other anatomical features (in addition to the cell wall density) are responsible for BI variability as well, particularly for earlywood blue intensity (EWBI), such as the lumen diameter' (Buckley et al., 2018, p. 14). The correlations made between EWBI, latewood blue intensity (LWBI), ΔBI (difference between EWBI and LWBI) and anatomical parameters (Figure 23) show that there is a correlation with the lumen diameter (ALL or ALW) of up to -0.562 (equal to the r between ALL and EWBI). Surprisingly, the correlation coefficient of EWBI and ALL is slightly higher than that of EWBI and eALL (-0.533).

The methodology used by Buckley to measure BI is explained in the section 'Blue intensity data'. It does not measure the BI of all pixels of the EW and LW but only a part of them and, therefore, a proxy of the minimum EW density and a proxy of the maximum LW density is measured. The fact that the final BI value does not correspond to the average value of all pixels affects the correlations with the wood anatomical parameters, which are calculated either on the area of the whole tree ring or only on EW or LW.
This procedure probably allows one to quickly exclude pixels that do not belong to the desired category (EW or LW), but it is an allocation based on BI and not on the definitions of EW and LW, which are based instead on the anatomical parameters of individual cells (Denne, 1988).

Although the concept of wood density has often been used for climate reconstruction, the comparisons between and within different methods to obtain insights about wood density remain rather complicated (Björklund et al., 2019).
The most widely used method in dendroclimatology to reconstruct the climate through wood density is to use X-ray microdensitometry. The maximum latewood density (MXD) parameter, measured by X-ray micro-densitometry, has indeed proven to have strong positive correlations with growing-season air temperature in temperate regions. The LWBI calculated by Buckley et al. (2018) would probably have a high correlation with the MXD measured on the same samples since the LWBI (as measured by Buckley et al. [2018]) is a proxy for the maximum latewood density (Björklund et al., 2019).
Analysing wood anatomy is emerging as a technique to extract information about wood density, but due to the large amount of time needed to do this kind of analysis, it is still not a very common method (Björklund et al., 2019).

The use of BI is a quick and low-cost approach to estimating wood density (Björklund et al., 2019) and is based on a principle known since the 1950s: lignin absorbs more ultraviolet light than other polysaccharide components, such as cellulose or hemicellulose (Fukazawa, 1992).

Lignin is a class of complex organic polymers and is the second most abundant biopolymer in the world, being present mainly in the cell walls of some plant cells (The Editors of Encyclopaedia Britannica, 2016). In conifers, the cell walls of tracheids consist of highly lignified primary walls and three-layered secondary cell walls. These last three layers are characterized by differences in thickness and lignification. Lignin is of crucial importance for the performance of the functions of the tracheids: reinforcing cell walls, facilitating water transport and preventing pathogens from entering the cell. Parenchyma cells may have less-lignified cell walls (Wagner et al., 2012).
The trigger of the lignification process is not yet known. The most intense phase of lignification takes place after the formation of the secondary wall and continues until the programmed cell death (apoptosis). In temperate climates, the most intense lignification period coincides with summer, but for LW cells, the process may end during the following spring, when the growth of a new ring has already begun. The process can take place at different rhythms even between adjacent cells (Wagner et al., 2012).

Through the correlation of intra-annual (e.g., monthly) climate data with BI data, a possible signal was obtained that refers to the period in which lignification takes place or a period in which a pre-conditioning necessary for lignification takes place. This signal may differ from a signal that can be obtained from the wood anatomical data, which refers to the period of cell formation or the period in which a pre-conditioning necessary for cell formation takes place.

Wood anatomical parameters and climate

When analysing the correlation coefficients of the correlations between the monthly precipitation data and the detrended data of the anatomical parameters divided by EW and LW cells, it emerges that the highest correlations for these two categories are in two different time periods.

For EW, the highest correlations are in the months of SON and OND. This result corresponds with the correlations found by Buckley et al. (2018) between EWBI and ΔBI of the same *Fokienia hodginsii* samples and precipitation: these two BI parameters show significant correlations for the prior October and November, even if those correlations are lower than those obtained in this thesis with the best anatomical parameters (eALA and ALA in particular). Consequently, the hypothesis of a pre-conditioning effect on the soil moisture by the autumn rainfall made by Buckley et al. (2018) is reinforced by the results of this thesis. The heavy rains that fall on Central Vietnam in autumn would mitigate the effects of the following dry season (January–April).

For LW were found less significant correlations between cell parameters and precipitation. The higher correlation (between AMJ precipitation and lALA) suggests that the LW is pre-conditioned by precipitation falling in late spring. Buckley et al. (2018) did not report any significant correlation between LWBI and a climatic parameter. This is therefore the first intra-annual indication of the growth period of LW cells in *Fokienia hodginsii*.

These correlations between precipitation and wood anatomical parameters give information at an intra-annual level on ring growth. In temperate zones, growing and dormancy seasons are well defined, but for tropical regions, this knowledge is not yet clearly established. EW of *Fokienia hodginsii* grows during or after the previous autumn's SON months, while LW grows during or after the AMJ months. It is not clear whether the effect of precipitation during these months is a pre-conditioning effect or actual conditioning during cell growth.

The parameters that best correlate with precipitation are the ALA and ALL parameters (either only in the EW, only in the LW or in the entire ring): water availability in the previous autumn is positively related to lumen area and length.

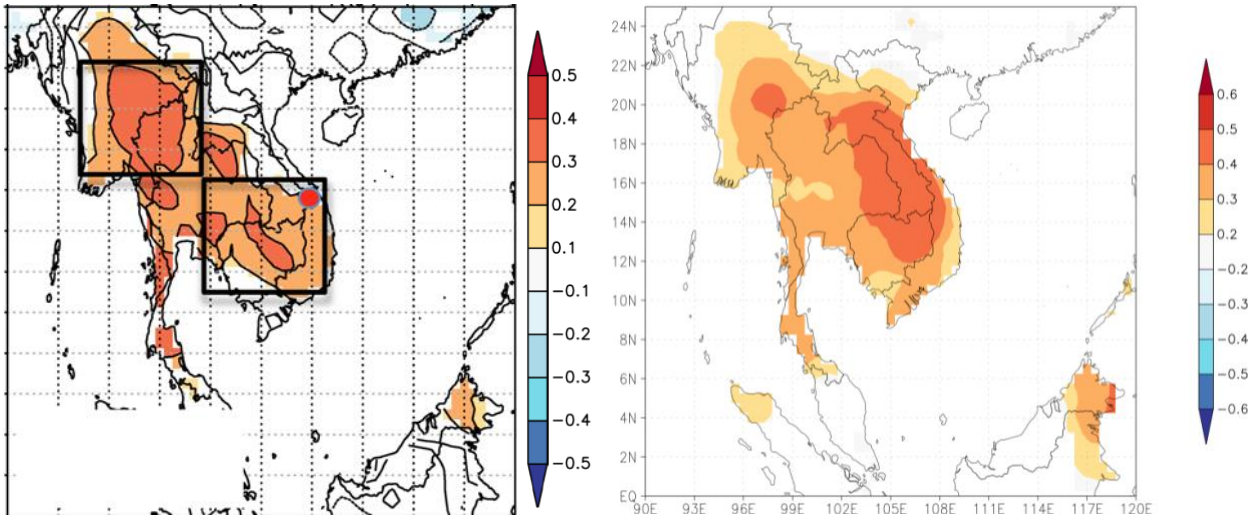

Figure 39: Comparison of the spatial correlation between April Standardized Precipitation Evapotranspiration Index (SPEI) data and ring width (on the left, from Buckley et al. [2017]) and ALP (on the right). The colour scale is different for the two images.

The analysis of the correlations with the monthly Standardized Precipitation Evapotranspiration Index (SPEI) data or the maximum monthly temperature confirms the importance of the month of April, already discussed by Buckley et al. (2017, 2018). For the EW, LW and the entire ring, there are anatomical parameters that correlate well and significantly with the April SPEI data. These correlations are higher than those between the April SPEI data and ring width (Figure 39).

During the months of MAM, the Intertropical Convergence Zone moves north through Southeast Asia and causes a rise in temperature and humidity. As a result, April is one of the warmest months in Southeast Asia. For most of Southeast Asia (with the exception of Central Vietnam), April is the month before the monsoon onset and therefore the month in which atmospheric drought is potentially at its peak (Buckley et al., 2018).

Correlations with the maximum monthly temperature give results similar to those of the SPEI data. It is interesting to note that the parameters that correlate best are the ALP (for the entire ring), the eALP (for the EW) and the AFC (for the LW) – exactly the same ones that correlate best with the April SPEI data.

The correlation between eALP and April maximum temperature is in the same order of magnitude as the one found by Buckley et al. (2018) between EWBI and December-to-April maximum temperature, with the difference that the latter is spatially more extended (Figure 40).

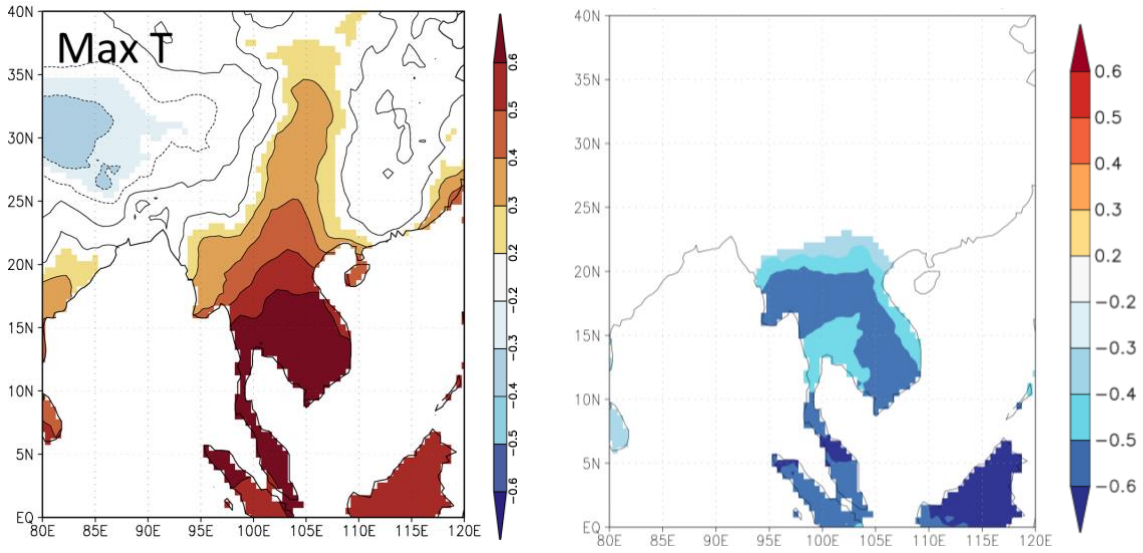

Figure 40: Correlation between earlywood blue intensity and December-to-April maximum temperature (1902–2013; Buckley et al., 2018; left) and between eALP and April maximum temperature (1970–2013). Only areas with significant correlation are shown.

The important dependence of both EW and LW parameters on the weather conditions of April allows to exclude that EW cells grow during the previous autumn. The effect of autumn precipitation is therefore confirmed as pre-conditioning.

The reconstructions made do not allow for conclusions with respect to the medium- or long–term trends of SON precipitation, the April maximum temperature and the April SPEI. However, other conclusions can be drawn. The linear models used for the climate reconstructions each have an R^2 between 0.18 and 0.22. This means that they explain 18%–22% of the data variance. This may seem rather low, but it is in line with the

result obtained in April SPEI reconstruction made by Buckley et al. (2017), where the model explained 23.3% of the variance.

In reconstructions made in other research on *Fokienia hodginsii*, however, the percentage of variance explained was much higher. Buckley et al. (2010) explain 35% of the Palmer Drought Severity Index variance, Buckley et al. (2018) 37% of the December-April maximum temperature variance and Buckley et al. (2019) even 57% of the Interdecadal Pacific Oscillation variance. The models developed in the papers cited, however, are based on a different type of detrending of the dendrochronological data and have passed measures of validation and improvement of the models, which was not the case for the reconstructions presented in this thesis.

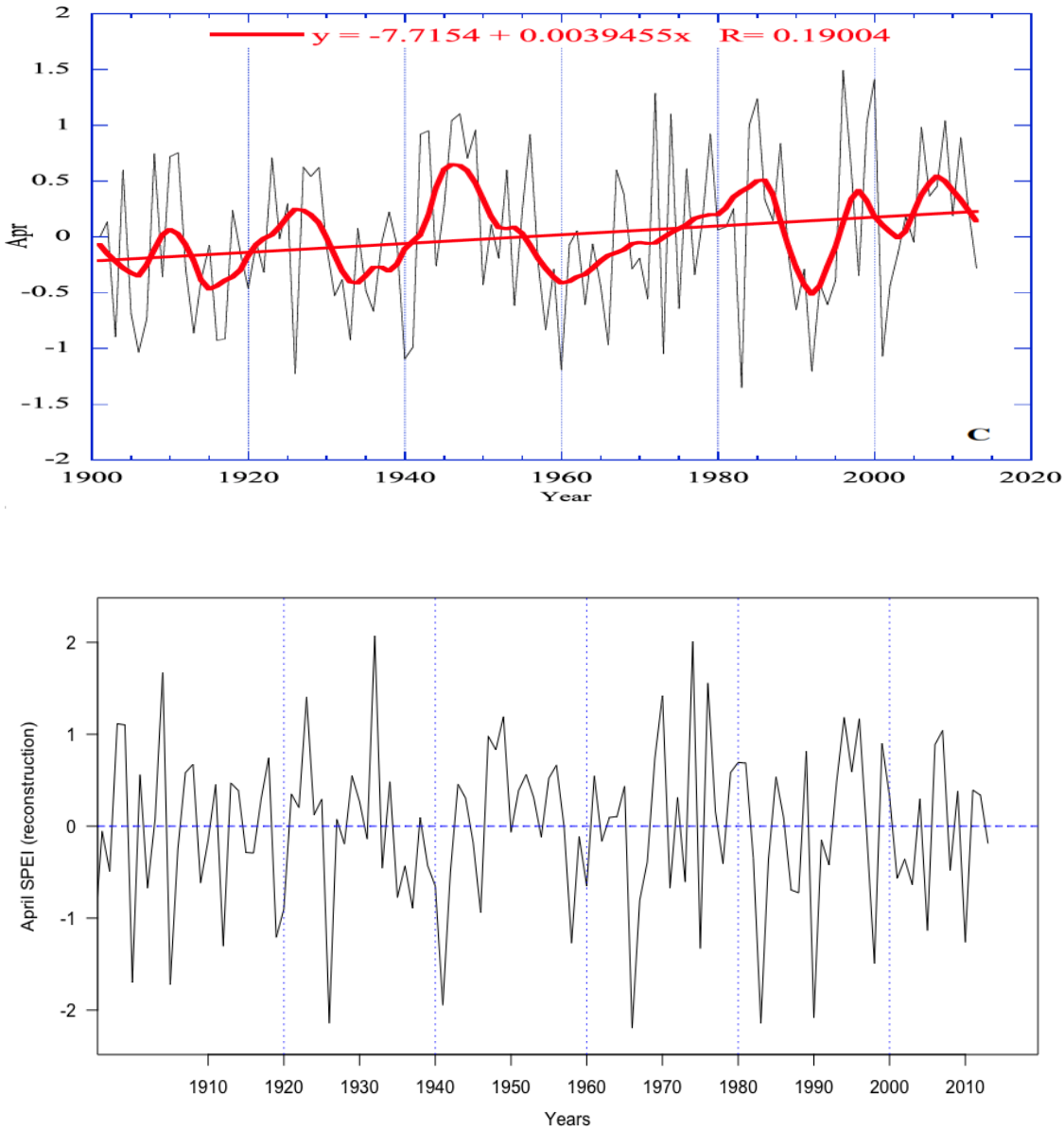

Figure 41: Reconstruction of the April SPEI data by Buckley et al. (2017; top) and of this thesis (bottom). The upper image is stretched to facilitate comparison with the lower image.

The reconstructions show large variations in climatic data from year to year and regularity in the occurrence of extreme climatic conditions.
The analysis of the 12 years with the most extreme climatic conditions for each reconstruction shows that in the years 1844–1845 and 1892–1893, the maximum temperatures in April were particularly low, while the SON rainfall was very high. The characteristics of these years are not reported in other studies.

The comparison between the reconstruction of the April SPEI data of Buckley et al. (2017) and that of this study shows clear similarities but also many differences. The differences are caused by two factors already mentioned: the methodology applied in the reconstruction and the type of detrending used. However, there is a very strong correspondence between the minimum and maximum peaks (Figure 41). The very dry years (SPEI negative) correspond particularly well in both plots (1905, 1926, 1941, 1966, 1975, 1983 and 1990). According to the reconstruction of SON precipitation, all the years with particularly low April SPEI data listed also had very low SON precipitation (< 4000 mm).

Limitations

The main limitation of this study is the reduced sample size. Despite the availability of numerous samples, the chronologies of anatomical parameters were obtained from only five cores. In addition, data have not been obtained for all tree rings for these five samples, and there are interruptions in the individual data series. This causes the wood anatomical parameter chronologies to be the results of the average of the detrended parameters of only one to three cores. The first reason that data were not obtained for all tree rings is that creating microslides and then digitizing and analysing is a time-consuming process, and the time available to write this thesis was limited. Secondly, due to the quality of the wood, the samples of *Fokienia hodginsii* were particularly difficult to process. Some of them broke during laboratory work.
Members of the Dendrosciences group at the WSL are developing techniques to reduce the complexity and the time needed to prepare large numbers of wood anatomical samples (Gärtner et al., 2014, 2015; Schneider & Gärtner, 2013). This research for technical improvement does not focus on a single step of the sampling preparation process but includes all the necessary steps to obtain anatomical images, from the core extraction to the cutting of microslides to scan techniques.

Another limitation of this study is due to the shape and size of the LW cells of *Fokienia hodginsii*. They have a very short lumen and a very small area. The goal of setting the filters in WinCELL was to find the best possible compromise to identify as many LW cells as possible but to try to include as few artefacts as possible (especially in EW). Consequently (as can also be seen in Figure 11), there may be cells identified with LW in EW and vice versa and cells in LW that have not been identified. This problem makes LW data slightly less reliable than EW data.

In addition, the method used to make climate reconstructions can be improved by introducing calibration and validation of the models. A combination of several dendrochronological variables (e.g., RW, eALP and EWBI) could also be used to reconstruct a single climate parameter.

Conclusions

This study demonstrates that wood anatomical parameters are a promising proxy for climate reconstruction in tropical areas. For the Vietnamese conifer *Fokienia hodginsii*, wood anatomical parameters show higher correlation with climate data than ring width does. This study supports the hypothesis of a pre-conditioning effect of the precipitation of the previous autumn and recognizes the importance of the month of April for xylem formation. Having analysed earlywood and latewood separately, this study has also been able to differentiate on an intra-annual scale which climatic conditions influence the formation of these two types of cells.

Further research should examine in depth and with a better sample size the relationship between climate and anatomical parameters for *Fokienia hodginsii* in other areas of Vietnam or Southeast Asia. Furthermore, the relation between climate and wood anatomical parameters in other tropical tree species should be explored. Finally, the content of the axial parenchyma cells should be studied chemically and functionally.
The methodology presents an important challenge that future studies must meet: providing excellent-quality microslides for wood anatomical studies. Accurate and scrupulous work is required in all steps, from sample collection to image analysis.

In an area such as Southeast Asia, where climate change will be particularly incidental and will have a strong impact on the daily lives of hundreds of millions of people, it is particularly important to understand the past climate to comprehend the extent of future changes. In the absence of valid and long climate measurements, it is necessary to reconstruct the climate using proxies such as ring width or wood anatomical parameters. Studying the response of tropical trees to climate is also important for developing optimal conservation policies to preserve tropical forests.

Acknowledgements

Foremost, I would like to thank my supervisor Prof. Dr. Paolo Cherubini for giving me the opportunity to work on a thesis that is in alignment with my interests. I am very grateful to have had the opportunity to work both in the laboratory and in the field, always aware of being supported and accompanied. I would like to thank him especially for the time he has made available and for not only following my thesis but for giving me an all-around scientific experience.

A special thanks goes also to Dr. Brendan Buckley, my co-supervisor, for the precious collaboration and for having made the field trip in Vietnam possible. The Southeast Asian Paleo Environments Consortium 2020, organized by him, was for me a great opportunity to interact with more experienced scientists from various scientific fields and to finally see the forests where *Fokienia hodginsii* grows. Thank you very much also to Mr. Le Canh Nam, who helped me a lot both in the field work in Vietnam and in the research of climate data.

From the WSL, I would like to thank Loïc Schneider, Dr. Marina Fonti, Anne Verstege, Dr. Richard Peters, Dr. Patrick Fonti and all the rest of the dendrosciences group for all their advice and technical support in the laboratory. A special thanks goes to Dr. Holger Gärtner for allowing me to participate in the International Course on Wood Anatomy and Tree-Ring Ecology 2019 in Klosters and for advising me during the analysis.

Literature

Baas, P., Ewers, F. W., Davis, S. D., & Wheeler, E. A. (2004). Evolution of xylem physiology. In *The evolution of plant physiology* (p. 512). Elsevier Ltd. https://doi.org/https://doi.org/10.1016/B978-0-12-339552-8.X5000-8

Baas, P., & Wheeler, E. A. (2011). Wood anatomy and climate change [Bookitem]. In *Climate Change, Ecology and Systematics* (pp. 141–155). Cambridge University Press. https://doi.org/10.1017/CBO9780511974540.007

Baas, Pieter, Blokhina, N., Fujii, T., Gasson, P. E., Grosser, D., Heinz, I., Ilic, J., Xiaomei, J., Miller, R., Newsom, L. A., Noshiro, S., Richter, H. G., Suzuki, M., Terrazas, T., Wheeler, E., & Wiedenhoeft, A. (2004). IAWA List of microscopic features for softwood identification. *IAWA Journal*, *25*(1), 1–70. https://doi.org/10.1163/22941932-90000349

Beguería, S., Vicente-Serrano, S. M., Reig, F., & Latorre, B. (2014). Standardized precipitation evapotranspiration index (SPEI) revisited: parameter fitting, evapotranspiration models, tools, datasets and drought monitoring [Article]. *International Journal of Climatology*, *34*(10), 3001–3023. https://doi.org/10.1002/joc.3887

Björklund, J., von Arx, G., Nievergelt, D., Wilson, R., Van den Bulcke, J., Günther, B., Loader, N. J., Rydval, M., Fonti, P., Scharnweber, T., Andreu-Hayles, L., Büntgen, U., D'Arrigo, R., Davi, N., De Mil, T., Esper, J., Gärtner, H., Geary, J., Gunnarson, B. E., … Frank, D. (2019). Scientific Merits and Analytical Challenges of Tree-Ring Densitometry. *Reviews of Geophysics*, *57*(4), 1224–1264. https://doi.org/10.1029/2019RG000642

Bryukhanova, M., & Fonti, P. (2013). Xylem plasticity allows rapid hydraulic adjustment to annual climatic variability. *Trees - Structure and Function*, *27*(3), 485–496. https://doi.org/10.1007/s00468-012-0802-8

Buckley, B. M., Anchukaitis, K. J., Penny, D., Fletcher, R., Cook, E. R., Sano, M., Nam, L. C., Wichienkeeo, A., Minh, T. T., & Hong, T. M. (2010). Climate as a contributing factor in the demise of Angkor, Cambodia. *Proceedings of the National Academy of Sciences of the United States of America*, *107*(15), 6748–6752. https://doi.org/10.1073/pnas.0910827107

Buckley, B. M., Fletcher, R., Wang, S. Y. S., Zottoli, B., & Pottier, C. (2014). Monsoon extremes and society over the past millennium on mainland Southeast Asia. *Quaternary Science Reviews*, *95*, 1–19. https://doi.org/10.1016/j.quascirev.2014.04.022

Buckley, B. M., Hansen, K. G., Griffin, K. L., Schmiege, S., Oelkers, R., D'Arrigo, R. D., Stahle, D. K., Davi, N., Nguyen, T. Q. T., Le, C. N., & Wilson, R. J. S. (2018). Blue intensity from a tropical conifer's annual rings for climate reconstruction: An ecophysiological perspective. *Dendrochronologia*, *50*(April), 10–22. https://doi.org/10.1016/j.dendro.2018.04.003

Buckley, B. M., Stahle, D. K., Luu, H. T., Wang, S. Y. S., Nguyen, T. Q. T., Thomas, P., Le, C. N., Ton, T. M., Bui,

T. H., & Nguyen, V. T. (2017). Central Vietnam climate over the past five centuries from cypress tree rings. *Climate Dynamics*, *48*(11–12), 3707–3723. https://doi.org/10.1007/s00382-016-3297-y

Buckley, B. M., Ummenhofer, C. C., D'Arrigo, R. D., Hansen, K. G., Truong, L. H., Le, C. N., & Stahle, D. K. (2019). Interdecadal Pacific Oscillation reconstructed from trans-Pacific tree rings: 1350–2004 CE. *Climate Dynamics*, *0*(0), 0. https://doi.org/10.1007/s00382-019-04694-4

Cherubini, P., Gartner, B. L., Tognetti, R., Bräker, O. U., Schoch, W., & Innes, J. L. (2003). Identification, measurement and interpretation of tree rings in woody species from mediterranean climates. *Biological Reviews of the Cambridge Philosophical Society*, *78*(1), 119–148. https://doi.org/10.1017/S1464793102006000

Crivellaro, A., & Schweingruber, F. H. (2013). Atlas of Wood, Bark and Pith Anatomy of Eastern Mediterranean Trees and Shrubs. In *Atlas of Wood, Bark and Pith Anatomy of Eastern Mediterranean Trees and Shrubs*. Springer Berlin Heidelberg. https://doi.org/10.1007/978-3-642-37235-3

Dallimore, W., Jackson, A. B., & Harrison, S. G. (1967). *A handbook of Coniferae and Ginkgoaceae* (St. Martin's Press (Ed.)).

Denne, M. P. (1988). Definition of latewood according to Mork (1928). *IAWA Journal*, *10*(1), 59–62.

Deutscher Wetterdienst. (2020). *Klimadaten ausgewählter Wetterstationen: Vietnam*. https://www.dwd.de/DE/leistungen/klimadatenwelt/asien/tz/vietnam/vietnam_node.html

Drought indices. (2020). Federal Office of Meteorology and Climatology MeteoSwiss. https://www.meteoswiss.admin.ch/home/climate/swiss-climate-in-detail/climate-indicators/drought-indices.html?param=rainanomaly

Eckstein, D. (2013). "A new star" - but why just parenchyma for dendroclimatology? *New Phytologist*, *198*(2), 328–330. https://doi.org/10.1111/nph.12229

El Niño-Southern Oscillation (ENSO). (n.d.). https://www.climate.gov/enso

Fritts, H. C. (1971). Dendroclimatology and dendroecology. *Quaternary Research*, *1*(4), 419–449. https://doi.org/10.1016/0033-5894(71)90057-3

Fukazawa, K. (1992). Ultraviolet Microscopy. In S. Y. Lin & C. W. Dence (Eds.), *Methods in Lignin Chemistry* (pp. 110–121). Springer Berlin Heidelberg. https://doi.org/10.1007/978-3-642-74065-7

Gärtner, H., Cherubini, P., Fonti, P., von Arx, G., Schneider, L., Nievergelt, D., Verstege, A., Bast, A., Schweingruber, F. H., & Büntgen, U. (2015). A technical perspective in modern tree-ring research - How to overcome dendroecological and wood anatomical challenges. *Journal of Visualized Experiments*, *2015*(97), 1–10. https://doi.org/10.3791/52337

Gärtner, H., Lucchinetti, S., & Schweingruber, F. H. (2014). New perspectives for wood anatomical analysis in dendrosciences: The GSL1-microtome. *Dendrochronologia*, *32*(1), 47–51. https://doi.org/10.1016/j.dendro.2013.07.002

Hacke, U. G., Lachenbruch, B., Pittermann, J., Mayr, S., Domec, J.-C., & Schulte, P. J. (2015). The Hydraulic

Architecture of Conifers. In U. G. Hacke (Ed.), *Functional and Ecological Xylem Anatomy* (pp. 39–75). Springer. https://doi.org/10.1007/978-3-319-15783-2

Harris, I., Osborn, T. J., Jones, P., & Lister, D. (2020). Version 4 of the CRU TS monthly high-resolution gridded multivariate climate dataset. *Scientific Data*, *7*(1), 1–18. https://doi.org/10.1038/s41597-020-0453-3

International Tree-ring Data Bank correlation statistics. (n.d.). ITRDB. Retrieved March 18, 2020, from ftp://ftp.ncdc.noaa.gov/pub/data/paleo/treering/measurements/correlation-stats/readme_correlation-stats.txt

Kaennel, M., & Schweingruber, F. H. (1995). *Multilingual glossary of dendrochronology : terms and definitions in English, German, French, Spanish, Italian, Portuguese and Russian* (Haupt (Ed.)). Swiss Federal Institute for Forest, Snow and Landscape Research.

Lamb, R. (1985). Vietnam Counts Forest and Species Loss after Years of War and Colonial Rule. *Ambio*, *14*(1), 62. http://www.jstor.org/stable/pdf/4313107.pdf?seq=1#page_scan_tab_contents

Lehejček, J., Buras, A., Svoboda, M., & Wilmking, M. (2017). Wood anatomy of Juniperus communis: a promising proxy for palaeoclimate reconstructions in the Arctic. *Polar Biology*, *40*(5), 977–988. https://doi.org/10.1007/s00300-016-2021-z

Liang, W., Heinrich, I., Simard, S., Helle, G., Liñán, I. D., & Heinken, T. (2013). Climate signals derived from cell anatomy of scots pine in NE Germany. *Tree Physiology*, *33*(8), 833–844. https://doi.org/10.1093/treephys/tpt059

Linderholm, H. W., Liu, Y., Leavitt, S. W., & Liang, E. (2013). Dendrochronology in Asia. *Quaternary International*, *283*, 1–2. https://doi.org/10.1016/j.quaint.2012.08.004

Liu, Y., Liang, P., & Sun, Y. (2019). Basic Features of the Asian Summer Monsoon System. In *The Asian Summer Monsoon* (pp. 3–22). Elsevier. https://doi.org/10.1016/b978-0-12-815881-4.00001-9

Morris, H. R. (2016). *The structure and function of ray and axial parenchyma in woody seed plants* (Issue July) [Ulm University]. https://doi.org/10.18725/OPARU-4087

Nguyen-Le, D., Matsumoto, J., & Ngo-Duc, T. (2014). Climatological onset date of summer monsoon in Vietnam. *International Journal of Climatology*, *34*(11), 3237–3250. https://doi.org/10.1002/joc.3908

O'Brien, M. J., Leuzinger, S., Philipson, C. D., Tay, J., & Hector, A. (2014). Drought survival of tropical tree seedlings enhanced by non-structural carbohydrate levels. *Nature Climate Change*, *4*(8), 710–714. https://doi.org/10.1038/nclimate2281

Peel, M. C., Finlayson, B. L., & McMahon, T. A. (2007). Updated world map of the K¨oppen-Geiger climate classification. *Hydrology and Earth System Sciences*, *11*, 1633–1644. https://doi.org/10.1002/ppp.421

Plavcová, L., & Jansen, S. (2015). The Role of Xylem Parenchyma in the Storage and Utilization of Nonstructural Carbohydrates. In U. G. Hacke (Ed.), *Functional and Ecological Xylem Anatomy* (pp. 209–234). Springer. https://doi.org/10.1007/978-3-319-15783-2

Pumijumnong, N. (2013). Dendrochronology in Southeast Asia. *Trees - Structure and Function*, *27*(2), 343–

358. https://doi.org/10.1007/s00468-012-0775-7

Räsänen, T. A., Lindgren, V., Guillaume, J. H. A., Buckley, B. M., & Kummu, M. (2016). On the spatial and temporal variability of ENSO precipitation and drought teleconnection in mainland Southeast Asia. *Climate of the Past*, *12*(9). https://doi.org/10.5194/cp-12-1889-2016

Robert, A. (2016). At the Heart of the Vietnam War: Herbicides, Napalm and Bulldozers Against the A Lưới Mountains. *Revue de Géographie Alpine*, *104–1*, 0–17. https://doi.org/10.4000/rga.3266

Robinson, W. J. (1990). Some historical background on dendrochronology. In *Methods of dendrochronology* (pp. 1–21). Springer. https://doi.org/10.1007/978-94-015-7879-0_1

Román-Jordán, E., Esteban, L. G., de Palacios, P., & Fernández, F. G. (2017). Comparative wood anatomy of the Cupressaceae and correspondence with phylogeny, with special reference to the monotypic taxa. *Plant Systematics and Evolution*, *303*(2), 203–219. https://doi.org/10.1007/s00606-016-1364-9

Rushforth, K. (2014). Notes on the Cupressaceae in Vietnam. *Tap Chi Sinh Hoc*, *29*(3), 32–39. https://doi.org/10.15625/0866-7160/v29n3.5384

Sano, M., Buckley, B. M., & Sweda, T. (2009). Tree-ring based hydroclimate reconstruction over northern Vietnam from Fokienia hodginsi: Eighteenth century mega-drought and tropical Pacific influence. *Climate Dynamics*, *33*(2–3), 331–340. https://doi.org/10.1007/s00382-008-0454-y

Sano, M., Xu, C., & Nakatsuka, T. (2012). A 300-year Vietnam hydroclimate and ENSO variability record reconstructed from tree ring δ18O. *Journal of Geophysical Research Atmospheres*, *117*(12), 1–11. https://doi.org/10.1029/2012JD017749

Schneider, L., & Gärtner, H. (2013). The advantage of using a starch based non-Newtonian fluid to prepare micro sections. *Dendrochronologia*, *31*(3), 175–178. https://doi.org/10.1016/j.dendro.2013.04.002

Schweingruber, F. H. (1988). *Tree Rings*. Springer Netherlands.

Schweingruber, F. H., Kairiukstis, L. A., & Shiyatov, S. (1990). Sample selection. In E. . Cook & L. A. Kairiukstis (Eds.), *Methods of dendrochronology: applications in the environmental sciences* (pp. 23–35).

Su, J., Gou, X., Deng, Y., Zhang, R., Liu, W., Zhang, F., Lu, M., Chen, Y., & Zheng, W. (2017). Tree growth response of Fokienia hodginsii to recent climate warming and drought in southwest China. *International Journal of Biometeorology*, *61*(12), 2085–2096. https://doi.org/10.1007/s00484-017-1409-y

The Editors of Encyclopaedia Britannica. (2016). *Lignin*. Encyclopædia Britannica. https://www.britannica.com/science/lignin

Thomas, P., & Yang, Y. (2013). Fokienia hodginsii , Fujian Cypress. In *The IUCN Red List of Threatened Species 2013*. http://dx.doi.org/10.2305/IUCN.UK.2013-1.RLTS.T32351A2815809.en

Trouet, V., & Van Oldenborgh, G. J. (2013). KNMI Climate Explorer: A Web-Based Research Tool for High-Resolution Paleoclimatology [Article]. *Tree-Ring Research*, *69*(1), 3–13. https://doi.org/10.3959/1536-1098-69.1.3

Von Arx, G., Crivellaro, A., Prendin, A. L., Čufar, K., & Carrer, M. (2016). Quantitative wood anatomy—practical

guidelines. *Frontiers in Plant Science*, *7*(JUNE2016), 1–13. https://doi.org/10.3389/fpls.2016.00781

Wagner, A., Donaldson, L., & Ralph, J. (2012). Lignification and Lignin Manipulations in Conifers. In L. Jouanin & C. Lapierre (Eds.), *Lignins: Biosynthesis, Biodegradation and Bioengineering* (1st ed., Vol. 61, pp. 37–76). Elsevier Ltd. https://doi.org/10.1016/B978-0-12-416023-1.00002-1

Worbes, M., & Fichtler, E. (2010). Wood Anatomy and Tree-Ring Structure and Their Importance for Tropical Dendrochronology. In W. J. Junk, F. Wittmann, P. Parolin, M. Piedade, & J. Schöngart (Eds.), *Amazonian Floodplain Forests: Ecophysiology, Biodiversity and Sustainable Management* (pp. 329–346). Springer. https://doi.org/10.1007/978-90-481-8725-6

Zheng, X. T. (2019). Indo-Pacific Climate Modes in Warming Climate: Consensus and Uncertainty Across Model Projections. *Current Climate Change Reports*, *5*(4), 308–321. https://doi.org/10.1007/s40641-019-00152-9

Ziaco, E., Biondi, F., & Heinrich, I. (2016). Wood cellular dendroclimatology: Testing new proxies in great basin bristlecone pine. *Frontiers in Plant Science*, *7*(OCTOBER2016), 1–13. https://doi.org/10.3389/fpls.2016.01602

Zuidema, P. A., Vlam, M., & Chien, P. D. (2011). Ages and long-term growth patterns of four threatened Vietnamese tree species. *Trees*, *25*(1), 29–38. https://doi.org/10.1007/s00468-010-0473-2

Appendix

Figures and tables

Table 10: Cores at WSL from the QNFH collection.

Tree name	Sample	First ring	Last ring	Years
TGFH3	A	1700	2010	310
TGFH4	C	1588	2013	425
TGFH10	A	1600	1967	367
	B	1550	2013	463
TGFH11	A	1600	2013	413
	B	1641	2013	372
	C	1670	2013	343
TGFH13	C	1550	1970	420
TGFH15	C	1568	1992	424
TGFH21	A	1643	2012	369
TGFH25	A	1600	2013	413
TGFH26	C	1720	1995	275
TGFH29	B	1573	2013	440
TGFH35	A	1650	1950	300
TGFH43	C	1680	2013	333
TGFH44	B	1620	2013	393
TGFH54	A	1644	1950	306
TGFH57	C	1634	2013	379
TGFH59	B	1560	2013	453
	C	1535	2013	478
TGFH60	B	1635	1992	357
	C	1700	1963	263

Table 11: Coefficients of correlation of the detrended wood anatomical parameters for the entire ring with the sum of the three-monthly rainfall (from September of the previous year). "Sum" corresponds to the sum of rainfall for the current year (January - December).

	RW1	RW2	%LA	ALA	ALL	ALW	ALP	AFC	ALLW
SON	0.2290	0.1344	0.4203*	0.4697*	0.4089*	0.3831*	0.4466*	-0.1376	0.1820
OND	0.3731	0.2795	0.4692*	0.4975*	0.4691*	0.3650	0.4505*	-0.0685	0.2528

NDJ	0.4076*	0.3240	0.3646	0.3426	0.3255	0.2251	0.2582	0.0028	0.2394
DJF	0.3928*	0.3200	0.4027*	0.3457	0.3373	0.2404	0.2177	0.1848	0.2364
JFM	0.1182	0.0924	0.3419	0.2529	0.2208	0.2253	0.1811	0.0548	0.0716
FMA	0.0570	0.0059	0.3074	0.2191	0.1827	0.1965	0.2356	-0.1425	0.0227
MAM	0.0118	0.0137	0.3630	0.2899	0.1965	0.3240	0.3320	-0.2326	0.0087
AMJ	0.2939	0.2899	0.2236	0.2376	0.1463	0.2967	0.2749	-0.1791	-0.0043
MJJ	0.0631	0.0983	0.1284	0.1625	0.0271	0.2933	0.1825	-0.1930	-0.1535
JJA	0.2903	0.3143	-0.1111	-0.0421	0.0050	-0.0906	-0.0779	0.1923	0.0280
JAS	-0.0335	-0.0717	0.0921	0.1353	0.1040	0.0890	0.0755	0.1245	0.0479
ASO	0.0742	0.0927	0.0706	0.1027	-0.0497	0.3309	-0.0576	0.4421*	-0.2449
Sum	0.1210	0.0997	0.3021	0.2661	0.1650	0.3415	0.1535	0.1752	0.0528

Table 12: Coefficients of correlation of the detrended wood anatomical parameters for earlywood with the sum of the three-monthly rainfall (from September of the previous year). "Sum" corresponds to the sum of rainfall for the current year (January – December).

	eALA	eALL	eALW	eACL	eALP	eAFC	eALLW	eAWT
SON	0.5393*	0.5000*	0.3359	0.4846*	0.4634*	-0.1437	0.2213	-0.1413
OND	0.5278*	0.5249*	0.2818	0.5041*	0.4483*	-0.1353	0.2706	-0.1719
NDJ	0.3744	0.3590	0.2035	0.3371	0.2742	-0.0778	0.1791	-0.1657
DJF	0.3172	0.3290	0.1331	0.2743	0.1908	0.0666	0.2027	-0.3373
JFM	0.2511	0.2410	0.1216	0.1807	0.2013	0.0164	0.1323	-0.3629
FMA	0.2397	0.2204	0.1317	0.1835	0.2752	-0.0962	0.0969	-0.2345
MAM	0.3279	0.1865	0.3290	0.1485	0.3889*	-0.2398	-0.0689	-0.2245
AMJ	0.2888	0.1190	0.3636	0.1108	0.3227	-0.1974	-0.1598	-0.0501
MJJ	0.2334	0.0162	0.3981*	0.0070	0.2501	-0.1996	-0.2636	-0.0494
JJA	-0.0214	0.0228	-0.0614	0.0586	-0.0312	0.1510	0.0432	0.1947
JAS	0.2068	0.2150	0.1022	0.2133	0.1405	0.1264	0.1476	-0.0403
ASO	0.1973	-0.0109	0.3994*	-0.0137	-0.0277	0.4919*	-0.2638	-0.0156
Sum	0.3183	0.1754	0.3440	0.1300	0.1598	0.1642	-0.0166	-0.2654

Table 13: Coefficients of correlation of the detrended wood anatomical parameters for latewood with the sum of the three-monthly rainfall (from September of the previous year). "Sum" corresponds to the sum of rainfall for the current year (January – December).

	lALA	lALL	lALW	lACL	lALP	lAFC	lALLW	lAWT
SON	0.1067	0.0975	0.0060	0.0842	0.2831	-0.3088	0.0152	0.0717
OND	0.1056	0.1819	-0.1107	0.1659	0.1746	-0.2318	0.1576	0.1415
NDJ	0.2187	0.3006	-0.1030	0.2841	0.0827	-0.0594	0.2918	0.2482

DJF	0.0622	0.1531	-0.1575	0.1459	-0.1220	0.0069	0.2770	0.1232
JFM	-0.0943	-0.0967	0.0085	-0.1446	-0.1064	-0.1048	-0.0249	-0.1566
FMA	-0.0426	-0.0950	0.0630	-0.1383	0.1092	-0.2725	-0.1084	-0.1468
MAM	0.1761	0.2042	0.0390	0.0833	0.2257	-0.2004	0.0852	0.0288
AMJ	0.4530*	0.4003*	0.1218	0.3186	0.3375	-0.0442	0.1484	0.2573
MJJ	0.3450	0.2431	0.1713	0.1343	0.2488	-0.0209	0.0106	0.0794
JJA	0.0670	0.1045	-0.0580	0.2109	-0.1658	0.2803	0.0930	0.2227
JAS	-0.2131	-0.1885	-0.1049	-0.0517	-0.1523	0.0033	-0.0234	0.0060
ASO	0.0862	-0.0169	0.3453	-0.0242	-0.0364	0.2560	-0.1785	-0.0196
Sum	0.0355	-0.0071	0.1475	-0.0308	0.0271	-0.0136	-0.0090	-0.0338

Table 14: Cores sampled during the field trip in Southern Vietnam, January 2020.

Tree name	**Sample**	**Date of sampling**	**Site**	**Elevation**
BDFH1	A	07.01.2020	12°11’01” N 108°41’31” E	1500 masl
	B			
BDFH2	A			
	B			
BDFH3B	B			
BDFH4	A			
	B			
BDFH5A	A	08.01.2020	12°11’23 N 108°42’45 E	1750 masl
BDFH6	A			
	B			
BDFH7	A			
	B			
BDFH8	A			
	B			
BDFH9	A			
	B			

Pictures of the SAPEC (Southeast Asian Paleo Environments Consortium) 2020

Bidoup Nui Ba National Park (BDNP), Lam Dong Province, Vietnam

January 4-12, 2020

Personal declaration

I hereby declare that the submitted thesis is the result of my own, independent work. All external sources are explicitly acknowledged in the thesis.